

Numerical Methods for the Hyperbolic Monge-Ampère Equation Based on the Method of Characteristics

M.W.M.C. Bertens^{1,*}, E.M.T. Vugts¹, M.J.H. Anthonissen¹,
J.H.M. ten Thije Boonkkamp¹, and W.L. IJzerman^{1,2}

¹*CASA, Department of Mathematics and Computer Science, Eindhoven University of Technology, PO Box 513, 5600 MB Eindhoven, The Netherlands*

²*Signify Research, High Tech Campus 7, 5656 AE Eindhoven, The Netherlands*

**Corresponding author: m.w.m.c.bertens@tue.nl*

Keywords— Numerical Solvers, Hyperbolic PDE, Method of Characteristics, Monge-Ampère

Abstract

We present three alternative derivations of the method of characteristics (MOC) for a second order nonlinear hyperbolic partial differential equation. The MOC gives rise to two mutually coupled systems of ordinary differential equations. As a special case we consider the Monge-Ampère (MA) equation, for which we solve the system of ODE's using explicit one-step methods (Euler, Runge-Kutta) and spline interpolation. Numerical examples demonstrate the performance of the methods.

1 Introduction

The general Monge-Ampère equation for a variable u in two independent variables x, y is of the form

$$A(u_{xx}u_{yy} - u_{xy}^2) + Bu_{xx} + Cu_{xy} + Du_{yy} + E = 0, \quad (1)$$

where A, B, C, D and E are functions, possibly dependent on x, y, u, u_x and u_y . The linearity in the Hessian $u_{xx}u_{yy} - u_{xy}^2$ is the defining feature of the Monge-Ampère equation. Applications of the Monge-Ampère equation are found, a.o., in fluid dynamics to compute the velocity of an incompressible fluid from the pressure using the streamline formulation [1], in mathematical finance to determine optimal portfolio strategies [2] and in Riemannian geometry to compute the surface of a manifold given the Gauss curvature [3].

Our interest lies in designing freeform optical surfaces, i.e., mirrors or lenses without any symmetries, to transfer a given light source distribution to a desired target distribution for some optical systems. Combining the optical map, i.e., the relation between a point in the source domain and a point in the target domain, with conservation of energy gives rise to two variants of the Monge-Ampère equation, viz. the elliptic and the hyperbolic equation [4]. The elliptic equation is well

established in the literature and used in optical design [4–7]. On the other hand, the hyperbolic equation is more exotic and the literature is scarce. The papers [8,9] are the most notable references in the context of numerical results in illumination optics, and the papers [10,11] are the most important results regarding existence and uniqueness results. It is conjectured that designing optical systems using the hyperbolic equation allows for the construction of more compact optics.

The hyperbolic Monge-Ampère equation has proven to be more difficult to solve than its elliptic counterpart. This is due to the existence of two mutually coupled families of characteristics. The two characteristics through an interior point (x_0, y_0) facing back to the boundary enclose the domain of dependence of this point. The solution $u(x_0, y_0)$ depends on all function values $u(x, y)$ with (x, y) in this domain. Conversely, the characteristics emanating from (x_0, y_0) bound the region of influence of (x_0, y_0) , which is the region where the solution is determined by $u(x_0, y_0)$. Figure 1 shows one such example where the blue and black lines indicate (a few of the) characteristics, where $(x_0, y_0) = (0.363, -0.167)$ which is denoted by the black dot and where the red and yellow parts indicate the domain of dependence and the domain of influence, respectively. Hence, boundary data determine the solution in the interior domain, and vice versa. Therefore, we distinguish between entering and leaving characteristics and fix a so-called initial strip, determined by a chosen parameterization, on which we prescribe Cauchy conditions. The remaining boundary conditions then follow from the course of the characteristics, by considering the domain of dependence, i.e., by considering where along the boundary, the characteristics enter or leave the domain. Depending on the number of characteristics entering and leaving, we can either solely prescribe u , prescribe u and the normal derivative of u , or we should not specify any boundary conditions at all. Therefore, it is of utmost importance that a numerical solution procedure is able to accurately approximate the location of the characteristics and identify the correct boundary conditions. In other words, a numerical method that violates either one of these conditions will completely destroy the solution.

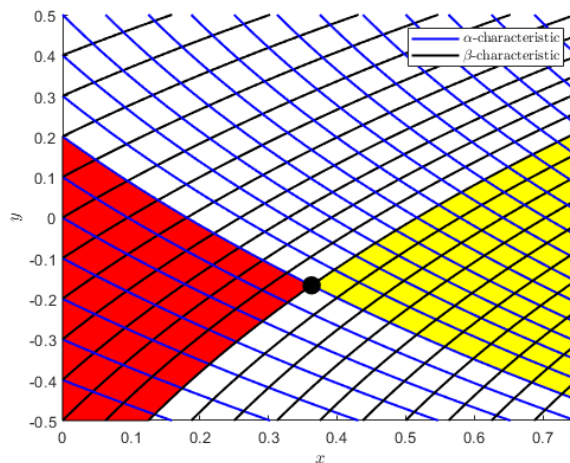


Figure 1: Schematic representation of domain of dependence (red) and domain of influence (yellow).

To start with, we introduce a general framework for second order nonlinear hyperbolic PDEs and subsequently restrict ourselves to the special case of the standard

hyperbolic Monge-Ampère equation, viz.

$$u_{xx}u_{yy} - u_{xy}^2 + f^2 = 0, \quad (2)$$

where f is a given continuously differentiable function dependent on x and y . The method of characteristics gives rise to two mutually coupled ODE systems, which we integrate with standard explicit one-step methods in the x -direction. Unfortunately, the direction of one characteristic depends on the other and vice versa, and characteristics do not necessarily pass from a numerical grid line to the next. Therefore missing information on a characteristic and in the grid points is obtained by spline interpolation. In order to control the interpolation error, we control the displacement of the characteristics in the y -direction by tuning the step size in the x -direction. This consequently determines the numerical domain of dependence, which is defined similar to the regular domain of dependence, but is formed by the numerical approximations of the characteristics instead. Furthermore, for a scheme for a hyperbolic PDE to be numerically stable, the (physical) domain of dependence should be enclosed by the numerical domain of dependence [12, p. 366]. By appropriately interpolating only within the area enclosed by the numerical characteristics and by step size control, the analytical domain of dependence lies within the domain of dependence of the numerical scheme and the developed schemes are stable in practice.

Estimates for the rate of convergence of the numerical methods are made, and tested for a variety of examples. We measure the convergence indirectly because direct measures are generally infeasible as they rely on analytical solutions, which are often unavailable. We do so by reformulating the Monge-Ampère equation as an integral equation and measuring its residual via Gauss-Legendre quadrature rules. We present examples which confirm u to be a saddle surface, one example where the number of required boundary conditions varies along the boundary, and one example with discontinuous third derivatives, for which no analytical solution is known.

We have organized our paper as follows. The theoretical framework for a hyperbolic second order PDE is introduced in Section 2. In Section 3 we apply this to the hyperbolic Monge-Ampère equation, and discuss the boundary conditions. Subsequently, we introduce the numerical methods in Section 4. In Section 5, various numerical results are given and analyzed, and finally a brief discussion and concluding remarks are given in Section 6.

2 Method of characteristics for a second order nonlinear hyperbolic PDE

We start by introducing the method of characteristics for a general nonlinear second order PDE in two variables. To this end we assume, unless explicitly stated otherwise, that all functions are continuous and have continuous derivatives of all orders involved. Let the PDE of interest be given by

$$F(x, y, u, p, q, r, s, t) = 0, \quad (x, y) \in \Omega, \quad (3)$$

where $u = u(x, y)$, $p = u_x$, $q = u_y$, $r = u_{xx}$, $s = u_{xy}$, $t = u_{yy}$ and $\Omega \subseteq \mathbb{R}^2$ the domain of interest.

2.1 An introduction to the method of characteristics

In this section we give a brief introduction to the method of characteristics.

Let C_b be a curve in the (x, y) -plane, parameterized by $\lambda \in I$, for an interval $I \subset \mathbb{R}$, i.e., $C_b = \{(X(\lambda), Y(\lambda)) | \lambda \in I\}$ with $X, Y : I \rightarrow \mathbb{R}$. Let C_0 be a corresponding curve in (x, y, z) -space, which we also parameterize by $\lambda \in I$, i.e., $C_0 = \{(X(\lambda), Y(\lambda), U(\lambda)) | \lambda \in I\}$ where $U : I \rightarrow \mathbb{R}$. The projection of C_0 on the (x, y) -plane yields the curve C_b , see Figure 2. We call C_b the base curve of C_0 , or simply the base curve.

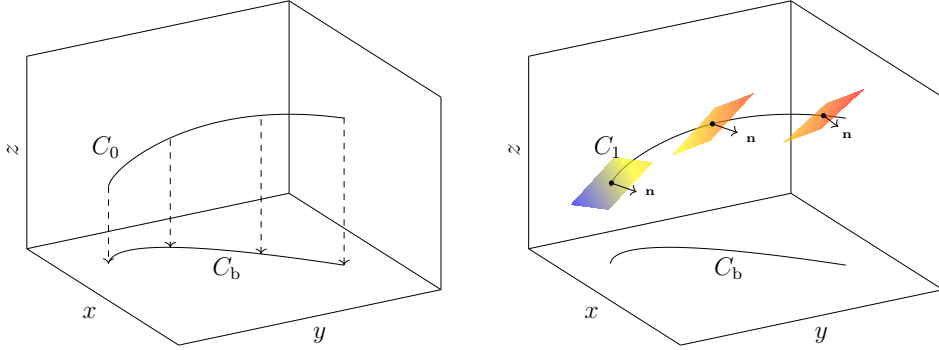


Figure 2: Schematic representation of the curves C_b , C_0 and the C_1 -strip. Three tangent planes and their normal vectors \mathbf{n} are drawn.

A base curve C_b is said to be differentiable if the corresponding map $\lambda \mapsto (X(\lambda), Y(\lambda))$ is differentiable for every $\lambda \in I$. A curve is regular if it is differentiable and the tangent vector has non-zero length for all $\lambda \in I$. We generally assume C_b to be regular, implying that $\frac{d}{d\lambda}(X(\lambda), Y(\lambda))^T \neq \mathbf{0}$, or equivalently $X_\lambda^2 + Y_\lambda^2 \neq 0$ for all $\lambda \in I$, where a subscript denotes differentiation.

Let $\mathbf{v} = (X_\lambda, Y_\lambda, U_\lambda)^T$ be the tangent vector to $(X(\lambda), Y(\lambda), U(\lambda)) \in C_0$ with $\lambda \in I$. A plane through the point $(X(\lambda), Y(\lambda), U(\lambda))$ with normal vector \mathbf{n} is tangent to the curve C_0 if $\mathbf{v} \cdot \mathbf{n} = 0$. To identify those planes let $\mathbf{n} = (P, Q, -1)^T$ with $P, Q : I \rightarrow \mathbb{R}$. Note that if the third component $n_3 \neq 0$, \mathbf{n} can always be reduced to such form by scaling the components. If for each point on C_0 we fix the tangent plane, then the collection of C_0 together with said tangent planes forms a so-called C_1 -strip, i.e.,

$$C_1 = \{(X(\lambda), Y(\lambda), U(\lambda), P(\lambda), Q(\lambda)) | \lambda \in I\}, \quad (4)$$

sometimes referred to as a strip of first order. Figure 2 shows the C_1 -strip for three tangent planes with corresponding normals. We use the notation C_1 interchangeably to denote either the strip's type, or the strip itself as given by (4). From $\mathbf{v} \cdot \mathbf{n} = 0$ it follows that

$$PX_\lambda + QY_\lambda - U_\lambda = 0, \quad (5)$$

which is the strip condition of first order, in short, the strip condition. Note that so far the C_1 -strip and the strip condition have no connection to the PDE (3).

Let $u(x, y)$ be a solution of (3), then $z = u(x, y)$ is called an integral surface of (3). An integral surface $z = u(x, y)$ naturally induces a C_1 -strip. Given a base curve C_b , let $u(\lambda) := u(X(\lambda), Y(\lambda))$, $p(\lambda) := p(X(\lambda), Y(\lambda))$ and $q(\lambda) := q(X(\lambda), Y(\lambda))$.

The normal of the integral surface $u(x, y) - z = 0$ is given by $\mathbf{n} = (u_x, u_y, -1)^T$ in (x, y, z) -space. Hence the strip $C_1 = \{(x(\lambda), y(\lambda), u(\lambda), p(\lambda), q(\lambda)) | \lambda \in I\}$ is obtained. From the chain rule we conclude

$$u_\lambda = u_x X_\lambda + u_y Y_\lambda = p X_\lambda + q Y_\lambda. \quad (6)$$

which is identical to the strip condition (5) with $P = p = u_x$, $Q = q = u_y$ and $U = u$, the solution of (3).

One can naturally generalize first order strips to higher order strips. A C_2 -strip consists of the C_1 -strip together with the tangent planes of the curves $(X(\lambda), Y(\lambda), P(\lambda))$ and $(X(\lambda), Y(\lambda), Q(\lambda))$. Higher order strip conditions are also found naturally in the following way: with $(X(\lambda), Y(\lambda), P(\lambda))$ we can associate two functions $R, S : I \rightarrow \mathbb{R}$ such that the normal vector of a tangent plane is $(R, S, -1)$. The tangent vector of $(X(\lambda), Y(\lambda), P(\lambda))$ equals $(X_\lambda, Y_\lambda, P_\lambda)$. The same reasoning as before applies and we find

$$P_\lambda = R X_\lambda + S Y_\lambda. \quad (7)$$

Analogously, for $(X(\lambda), Y(\lambda), Q(\lambda))$ let the normal vector of a tangent plane be $(\tilde{S}, T, -1)$, it then follows that

$$Q_\lambda = \tilde{S} X_\lambda + T Y_\lambda. \quad (8)$$

Note that the functions S and \tilde{S} are not necessarily equal as $(R, S, -1)^T$ should be perpendicular to the curve $(X_\lambda, Y_\lambda, P_\lambda)$ and $(\tilde{S}, T, -1)^T$ should be perpendicular to the curve $(X_\lambda, Y_\lambda, Q_\lambda)$. As before, an integral surface $z = u(x, y)$ induces a C_2 -strip where we identify Q, R, S, \tilde{S} and T with the values r, s, t via $R = r = u_{xx}(X(\lambda), Y(\lambda))$, $S = s = u_{xy}(X(\lambda), Y(\lambda))$, $\tilde{S} = \tilde{s} = u_{yx}(X(\lambda), Y(\lambda))$ and $T = t = u_{yy}(X(\lambda), Y(\lambda))$. We assume u is twice continuously differentiable, and therefore $S = u_{xy} = u_{yx} = \tilde{S}$. Henceforth strip conditions of second order for u become

$$p_\lambda = r X_\lambda + s Y_\lambda, \quad (9a)$$

$$q_\lambda = s X_\lambda + t Y_\lambda. \quad (9b)$$

For completeness we give the strip conditions of third order, viz.,

$$r_\lambda = u_{xxx} X_\lambda + u_{xxy} Y_\lambda = r_x X_\lambda + r_y Y_\lambda = r_x X_\lambda + s_x Y_\lambda, \quad (10a)$$

$$s_\lambda = u_{xyx} X_\lambda + u_{xyy} Y_\lambda = s_x X_\lambda + s_y Y_\lambda = s_x X_\lambda + t_x Y_\lambda = r_y X_\lambda + s_y Y_\lambda, \quad (10b)$$

$$t_\lambda = u_{yyx} X_\lambda + u_{yyy} Y_\lambda = t_x X_\lambda + t_y Y_\lambda = s_y X_\lambda + t_y Y_\lambda. \quad (10c)$$

The process of finding higher order strips is called extending. To clarify, the curve $C_0 = \{(X(\lambda), Y(\lambda), U(\lambda)) | \lambda \in I\}$ (a strip of zeroth order) is extended to a strip C_1 , given by (4). Similarly C_1 is extended to a strip of second order, given by

$$C_2 = \{(X(\lambda), Y(\lambda), U(\lambda), P(\lambda), Q(\lambda), R(\lambda), S(\lambda), \tilde{S}(\lambda), T(\lambda)) | \lambda \in I\}. \quad (11)$$

We define C_2 to be an integral strip if there exists a C_1 -strip which can be extended to the C_2 -strip uniquely, solely using the PDE (3) and the strip conditions (9). In this case C_1 is called a *free strip*. If C_1 is not a free strip, additional requirements should be prescribed in order for C_1 to be extendable to an integral

strip C_2 . In this case we call C_1 a *characteristic strip* which implies that not all second order derivatives of u can be determined uniquely from C_1 , the PDE (3) and the strip conditions. To put into context, let $C_b = \{(x(\lambda), y(\lambda)) | \lambda \in I\}$ be a base curve, $z = u(x, y)$ be an integral surface of (3) and let C_0 be a corresponding zeroth order strip. Furthermore, we supplement $p = u_x$ and $q = u_y$ to obtain a first order strip C_1 . If by using the PDE (3) and the strip conditions (9) we are able to determine $r = u_{xx}$, $s = u_{xy}$ and $t = u_{yy}$ uniquely, then the strip $C_2 = \{(x(\lambda), y(\lambda), u(\lambda), p(\lambda), q(\lambda), r(\lambda), s(\lambda), t(\lambda)) | \lambda \in I\}$ is called an integral strip, and C_1 is a free strip, otherwise C_1 is called a characteristic strip.

Note that along a free strip, but not along a characteristic strip, the derivatives u_{xx} , u_{xy} and u_{yy} can all be determined along the strip, either by being interior derivatives with respect to C_1 , or by combining the PDE (3) with the remaining interior derivatives. To illustrate, given u , $p = u_x$ and $q = u_y$, on a vertical line segment, i.e., $X_\lambda = 0$, by differentiation with respect to y one can obtain u_{xy} and u_{yy} , and u_{xx} follows from the PDE, as will be shown in Section 3.1.

For completeness, if C_1 is a characteristic strip, its carrier C_0 will be called a characteristic curve in (x, y, z) -space, and the base curve C_b , will be called a characteristic base curve. Generally we refer to a characteristic strip, characteristic curve and characteristic base curve simply as ‘the characteristic’.

Note that thus far we considered an entire curve/strip to be either free or characteristic. Formally this should be evaluated pointwise, which introduces the notion of a characteristic base point, a characteristic point and a characteristic element for a 2-, 3- and 5-dimensional point on C_b , C_0 and C_1 , respectively. This distinction is often not necessary due to the fact that every strip, which has one point in common with the integral surface and all its tangent planes equal to that of the integral surface, lies entirely on said surface. To see this consider the strip γ parameterized by $\lambda \in I$, given by $\gamma(\lambda) = (X(\lambda), Y(\lambda), U(\lambda), u_x(\lambda), u_y(\lambda))$ with strip condition $U_\lambda = u_x X_\lambda + u_y Y_\lambda$. Let (x_0, y_0, u_0) lie on the integral surface $z = u(x, y)$, so $u_0 = u(x_0, y_0)$. Furthermore, let γ pass through (x_0, y_0, u_0) , i.e., there exists a λ_0 such that $(x_0, y_0, u_0) = (X(\lambda_0), Y(\lambda_0), U(\lambda_0))$ and $u_0 = u(X_0, Y_0) = u(X(\lambda_0), Y(\lambda_0))$. Let $d(\lambda) = U(\lambda) - u(X(\lambda), Y(\lambda))$ be the pointwise signed vertical distance between the integral surface $z = u(x, y)$ and the strip γ at the point $(X(\lambda), Y(\lambda), u(X(\lambda), Y(\lambda)))$. If $d \equiv 0$ then clearly γ lies on the integral surface $z = u(x, y)$. Obviously it holds that $d(\lambda_0) = 0$. Furthermore, the change in the signed distance d for $\lambda \in I$ can be found by

$$\frac{dd}{d\lambda} = \frac{dU}{d\lambda} - u_x \frac{dX}{d\lambda} - u_y \frac{dY}{d\lambda} = \frac{dU}{d\lambda} - (u_x X_\lambda + u_y Y_\lambda) = \frac{dU}{d\lambda} - U_\lambda = 0, \quad (12)$$

where we applied the strip condition. Because $\frac{dd}{d\lambda} = 0$ for all $\lambda \in I$ and $d(\lambda_0) = 0$, $d \equiv 0$, and hence the strip lies entirely on the integral surface u .

2.2 The characteristic condition

We will derive and discuss the conditions under which a strip C_1 is a characteristic strip in this section. These conditions will be called the characteristic conditions. We will impose conditions on C_1 , based on our starting equation (3), such that (at least one of the) second and higher order derivatives cannot be determined uniquely. We will discuss three different approaches to obtaining the characteristic conditions.

2.2.1 The characteristic condition by the implicit function theorem

Fundamentally, we are looking for conditions on the solvability for the second order derivatives r , s and t . One way to derive the characteristic condition is to apply the implicit function theorem. To this end, let the C_1 -strip be parameterized by λ as before. Define

$$\mathbf{f}(x, y, u, p, q, x_\lambda, y_\lambda, p_\lambda, q_\lambda \mid r, s, t) = \begin{pmatrix} F(x, y, u, p, q, r, s, t) \\ x_\lambda r + y_\lambda s - p_\lambda \\ x_\lambda s + y_\lambda t - q_\lambda \end{pmatrix}. \quad (13)$$

The components of the vector-valued function \mathbf{f} are formed by our PDE (3) and the two strip conditions (9) for p_λ and q_λ . The implicit function theorem [13, p. 731] states that if there exists a λ_0 such that

$$\begin{aligned} \mathbf{f}(x(\lambda_0), y(\lambda_0), u(\lambda_0), p(\lambda_0), q(\lambda_0), x_\lambda(\lambda_0), y_\lambda(\lambda_0), \\ p_\lambda(\lambda_0), q_\lambda(\lambda_0) \mid r(\lambda_0), s(\lambda_0), t(\lambda_0)) = \mathbf{0}, \end{aligned} \quad (14)$$

and the Jacobi matrix

$$\mathbf{A} := \frac{\partial \mathbf{f}}{\partial (r, s, t)} = \begin{pmatrix} F_r & F_s & F_t \\ x_\lambda & y_\lambda & 0 \\ 0 & x_\lambda & y_\lambda \end{pmatrix}, \quad (15)$$

is nonsingular, then there is an open set $\Lambda \subset \mathbb{R}$ containing λ_0 and a unique continuously differentiable function $\mathbf{g} : \Lambda \rightarrow \mathbb{R}^3$ with $\mathbf{g}(\lambda_0) = (r(\lambda_0), s(\lambda_0), t(\lambda_0))^T$ such that

$$\mathbf{f}(x(\lambda), y(\lambda), u(\lambda), p(\lambda), q(\lambda), x_\lambda(\lambda), y_\lambda(\lambda), p_\lambda(\lambda), q_\lambda(\lambda) \mid \mathbf{g}(\lambda)) = \mathbf{0}, \text{ for all } \lambda \in \Lambda. \quad (16)$$

If $D := \det(\mathbf{A}) \neq 0$, then (r, s, t) can be found uniquely along C_1 , i.e., we have a free strip. Alternatively, if $D = 0$, then (r, s, t) cannot be determined uniquely, hence we have a characteristic strip. The case $D = 0$ is therefore called the characteristic condition and it can be written as

$$D = F_r y_\lambda^2 - F_s x_\lambda y_\lambda + F_t x_\lambda^2 = 0. \quad (17)$$

2.2.2 The characteristic condition by a coordinate transformation

The characteristic condition can also be derived by means of a coordinate transformation [14, p. 419] This can be achieved due to the following equivalent definition of a characteristic. If the differential equation $F = 0$ represents an interior differential equation along a strip C_1 , then C_1 is a characteristic strip. The term interior differential operator here means that along C_1 the second order differential operator F can be expressed solely in terms of derivatives of x , y and u with respect to the parameter describing the base curve of C_1 .

Let C_1 be the strip of interest with corresponding base curve C_b as shown in Figure 3. We introduce the coordinate transformation

$$(x, y) \rightarrow (\phi(x, y), \lambda(x, y)), \quad (18)$$

where λ is the parameter along the curve C_b and ϕ leads away from C_b .

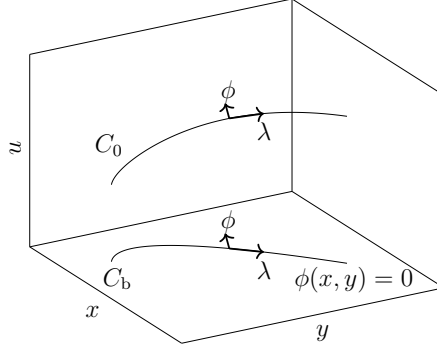


Figure 3: Schematic representation of a curve C_0 , with its base curve C_b and the accompanying parameters along and perpendicular to the curves.

Recall that we require C_b to be a regular curve, i.e., $x_\lambda^2 + y_\lambda^2 \neq 0$. Adopting the new coordinates the derivatives of u are:

$$u_x = u_\phi \phi_x + u_\lambda \lambda_x, \quad (19a)$$

$$u_y = u_\phi \phi_y + u_\lambda \lambda_y, \quad (19b)$$

$$u_{xx} = u_{\phi\phi} (\phi_x)^2 + 2u_{\phi\lambda} \phi_x \lambda_x + u_{\lambda\lambda} (\lambda_x)^2 + u_\phi \phi_{xx} + u_\lambda \lambda_{xx}, \quad (19c)$$

$$u_{xy} = u_{\phi\phi} \phi_x \phi_y + u_{\phi\lambda} (\phi_x \lambda_y + \phi_y \lambda_x) + u_{\lambda\lambda} \lambda_x \lambda_y + u_\phi \phi_{xy} + u_\lambda \lambda_{xy}, \quad (19d)$$

$$u_{yy} = u_{\phi\phi} (\phi_y)^2 + 2u_{\phi\lambda} \phi_y \lambda_y + u_{\lambda\lambda} (\lambda_y)^2 + u_\phi \phi_{yy} + u_\lambda \lambda_{yy}. \quad (19e)$$

Using these relations, one can construct a function G such that

$$F(x, y, u, u_x, u_y, u_{xx}, u_{xy}, u_{yy}) = G(\phi, \lambda, u, u_\phi, u_\lambda, u_{\phi\phi}, u_{\phi\lambda}, u_{\lambda\lambda}) = 0. \quad (20)$$

Recall that a C_1 -strip is characteristic if not all higher order derivatives can be determined uniquely along the strip. As p and q are known on a C_1 -strip, both u_ϕ and u_λ can be obtained provided the Jacobian of the coordinate transformation (18) $\phi_x \lambda_y - \phi_y \lambda_x \neq 0$. Because λ is the parameter along the strip, $(u_\phi)_\lambda$ and $(u_\lambda)_\lambda$ can naturally be found by differentiating along the strip. Therefore, for C_1 to be characteristic, $u_{\phi\phi}$ should be undetermined. If $G_{u_{\phi\phi}} = 0$ then $u_{\phi\phi}$ cannot be determined from $G = 0$. Hence differentiating (20) and applying (19c)-(19e) we find

$$\begin{aligned} G_{u_{\phi\phi}}(\phi, \lambda, u, u_\phi, u_\lambda, u_{\phi\phi}, u_{\phi\lambda}, u_{\lambda\lambda}) &= F_{u_{xx}} \frac{\partial u_{xx}}{\partial u_{\phi\phi}} + F_{u_{xy}} \frac{\partial u_{xy}}{\partial u_{\phi\phi}} + F_{u_{yy}} \frac{\partial u_{yy}}{\partial u_{\phi\phi}} \\ &= F_r \phi_x^2 + F_s \phi_x \phi_y + F_t \phi_y^2 \\ &= 0, \end{aligned} \quad (21)$$

which is the characteristic condition. Assuming $\phi_y \neq 0$, this can further be rewritten as

$$F_r \left(\frac{\phi_x}{\phi_y} \right)^2 + F_s \frac{\phi_x}{\phi_y} + F_t = 0. \quad (22)$$

To see that this is equivalent to (17) consider the following: ϕ is constant along C_b , therefore for fixed x, y it should not depend on λ , i.e.,

$$\phi_\lambda = \phi_x x_\lambda + \phi_y y_\lambda = 0, \quad (23)$$

which is equivalent to

$$\frac{\phi_x}{\phi_y} = -\frac{y_\lambda}{x_\lambda}. \quad (24)$$

Substituting this in (22) yields the previously found characteristic condition (17).

2.2.3 The characteristic condition for second order strips

In the previous sections we established relations such that C_1 is uniquely defined, while C_2 -strips are not. Although the characteristic condition $D = 0$ is fundamental, it yields no practical means to determine the evolution of the solution along a C_1 -strip. In this section we show that the characteristic condition obtained also holds for second order strips, which does provide insights on how to determine the evolution of a C_1 -strip. This evolution will be further discussed in Section 2.3 and Section 2.4.

Not all second order derivatives can be determined along a characteristic C_1 -strip. Likewise, not all third order derivatives can be determined uniquely either. To determine relations for the derivatives of r, s, t we apply strip conditions (10), together with additional relations, which are found by differentiating the PDE (3) with respect to x and y , viz.,

$$\frac{dF}{dx} = F_x + F_u p + F_p r + F_q s + F_r r_x + F_s s_x + F_t t_x = 0, \quad (25a)$$

$$\frac{dF}{dy} = F_y + F_u q + F_p s + F_q t + F_r r_y + F_s s_y + F_t t_y = 0. \quad (25b)$$

Combining these with strip conditions (10) with $X(\lambda) = x(\lambda)$ etc., yields two systems of equations

$$\mathbf{A} \begin{pmatrix} r_x \\ s_x \\ t_x \end{pmatrix} = \begin{pmatrix} -F^x \\ r_\lambda \\ s_\lambda \end{pmatrix}, \quad \mathbf{A} \begin{pmatrix} r_y \\ s_y \\ t_y \end{pmatrix} = \begin{pmatrix} -F^y \\ s_\lambda \\ t_\lambda \end{pmatrix}, \quad (26)$$

where the equations are formed by collecting the x - and y -derivatives respectively, and where $F^x := F_x + F_u p + F_p r + F_q s$, $F^y = F_y + F_u q + F_p s + F_q t$ and \mathbf{A} is given by (15). Because F becomes an interior operator along a characteristic strip, r_λ, s_λ and t_λ can be determined along a C_2 -strip while not all of r_x, s_x, t_x, r_y, s_y and t_y can. Therefore \mathbf{A} should be singular. Hence we obtain once more the characteristic condition (17).

2.3 Compatibility conditions

Because $D = \det(\mathbf{A}) = 0$, the systems in (26) may not have solutions. In this section we will derive compatibility conditions such that solutions do exist. Consider the rank of \mathbf{A} . The rank of a matrix equals the order of the largest non-vanishing

minor, which is known as the determinantal rank. The matrix \mathbf{A} has 9 minors of order 2, the minors formed by the lower right and lower left 2×2 submatrices are

$$M_{1,1} = \begin{vmatrix} y_\lambda & 0 \\ x_\lambda & y_\lambda \end{vmatrix} = y_\lambda^2, \quad M_{1,3} = \begin{vmatrix} x_\lambda & y_\lambda \\ 0 & x_\lambda \end{vmatrix} = x_\lambda^2, \quad (27)$$

where M_{ij} denotes the minor formed by deleting the i th row and j th column. Because $x_\lambda^2 + y_\lambda^2 \neq 0$, $M_{1,1}$ and $M_{1,3}$ cannot be 0 simultaneously, hence $D = 0$ implies $\text{rank}(\mathbf{A}) = 2$. From (26) we conclude that solutions $(r_x, s_x, t_x)^\top$ and $(r_y, s_y, t_y)^\top$ do not always exist if \mathbf{A} is singular. Therefore we require the left and right hand sides of (26) to be compatible, i.e., the vectors $(-F^x, r_\lambda, s_\lambda)^\top$ and $(-F^y, s_\lambda, t_\lambda)^\top$ should be in the column-space of any two columns of \mathbf{A} . Hence the matrix of any two column vectors of \mathbf{A} with either $(-F^x, r_\lambda, s_\lambda)^\top$ or $(-F^y, s_\lambda, t_\lambda)^\top$ should be singular. To this end we introduce the matrices

$$\mathbf{A}^x = \left(\begin{array}{ccc|c} F_r & F_s & F_t & -F^x \\ x_\lambda & y_\lambda & 0 & r_\lambda \\ 0 & x_\lambda & y_\lambda & s_\lambda \end{array} \right), \quad (28a)$$

$$\mathbf{A}^y = \left(\begin{array}{ccc|c} F_r & F_s & F_t & -F^y \\ x_\lambda & y_\lambda & 0 & s_\lambda \\ 0 & x_\lambda & y_\lambda & t_\lambda \end{array} \right). \quad (28b)$$

Let D_{klm}^x denote the determinant formed by selecting the columns k, l and m of \mathbf{A}^x and similarly, we introduce D_{klm}^y . We find by including the first, third and fourth column

$$D_{134}^x = \begin{vmatrix} F_r & F_t & -F^x \\ x_\lambda & 0 & r_\lambda \\ 0 & y_\lambda & s_\lambda \end{vmatrix} = -(F^x x_\lambda y_\lambda + F_r y_\lambda r_\lambda + F_t x_\lambda s_\lambda), \quad (29a)$$

$$D_{134}^y = \begin{vmatrix} F_r & F_t & -F^y \\ x_\lambda & 0 & s_\lambda \\ 0 & y_\lambda & t_\lambda \end{vmatrix} = -(F^y x_\lambda y_\lambda + F_r y_\lambda s_\lambda + F_t x_\lambda t_\lambda), \quad (29b)$$

which both should equal zero due to \mathbf{A} being singular. Trivially, since $D = 0$ similar calculations yield $D_{124}^x = D_{134}^x x_\lambda / y_\lambda$, $D_{234}^x = D_{134}^x y_\lambda / x_\lambda$, $D_{124}^y = D_{134}^y x_\lambda / y_\lambda$, $D_{234}^y = D_{134}^y y_\lambda / x_\lambda$ for $x_\lambda, y_\lambda \neq 0$.

Condition (17) turns out to be enough to determine the evolution of x, y, u, p and q along the characteristics. Conditions (29) are needed for the evolutions of other variables which are introduced in the next section.

2.4 Evolution along the characteristics

To derive the evolution of the solution along the characteristics we rewrite (17) as a second order polynomial equation, viz.

$$D(\mu) = F_r \mu^2 - F_s \mu + F_t = 0, \quad (30)$$

where we introduced $\mu = y_\lambda / x_\lambda$ assuming $x_\lambda \neq 0$. In case $x_\lambda = 0$, we can use $\tilde{\mu} = x_\lambda / y_\lambda$ instead. Solving (30) for μ yields two roots a and b viz.

$$a = \frac{F_s + \sqrt{\Delta}}{2F_r}, \quad b = \frac{F_s - \sqrt{\Delta}}{2F_r}, \quad (31)$$

where $\Delta = F_s^2 - 4F_r F_t$ is the discriminant. The discriminant allows us to classify the differential operator F . If at a point $\mathbf{x}_0 = (x_0, y_0) \in \Omega$ the discriminant $\Delta(\mathbf{x}_0) > 0$, then the PDE (3) is hyperbolic in that point [14, p. 420]. Naturally there exists a (small) neighborhood of \mathbf{x}_0 for which the PDE is hyperbolic. Similarly we call the PDE parabolic in \mathbf{x}_0 if $\Delta(\mathbf{x}_0) = 0$ and elliptic if $\Delta(\mathbf{x}_0) < 0$. If for all $\mathbf{x}_0 \in \Omega$ we have $\Delta(\mathbf{x}_0) > 0$, then F is called hyperbolic, or hyperbolic in the entire domain. In the following we restrict ourselves to the hyperbolic case. By definition, we have two separate families of characteristic curves defined by $a(x(\lambda), y(\lambda))x_\lambda = y_\lambda$ or $b(x(\lambda), y(\lambda))x_\lambda = y_\lambda$, respectively, passing through the point $(x(\lambda), y(\lambda))$.

We can express F_r, F_s and F_t in terms of a, b and Δ using (31) as

$$F_t = \frac{ab}{a-b}\sqrt{\Delta}, \quad F_s = \frac{a+b}{a-b}\sqrt{\Delta}, \quad F_r = \frac{1}{a-b}\sqrt{\Delta}. \quad (32)$$

Alternatively, we can express a and b in terms of F_r, F_s and F_t as

$$a+b = \frac{F_s}{F_r}, \quad ab = \frac{F_t}{F_r}. \quad (33)$$

Using the definition of μ we find $y_\lambda/x_\lambda = a$ or $y_\lambda/x_\lambda = b$, implying we have two distinct families of characteristics, one induced by a , and the other induced by b . To distinguish the characteristics, we write $x = x(\alpha)$, $y = y(\alpha)$ and $x = x(\beta)$, $y = y(\beta)$ for the characteristic induced by a and b , respectively. Henceforth α and β effectively take over the role of λ . As such instead of x_λ we write $\frac{dx}{d\alpha} = x_\alpha$ for the derivative of x with respect to α , and similarly for the other variables and for differentiation with respect to β .

The matrix \mathbf{A} , given in (15) actually represents two distinct matrices, \mathbf{A}^α and \mathbf{A}^β , because the derivatives w.r.t. λ can be associated with both α and β . Because further derivations for either characteristic is done analogously for the other, we will only treat the characteristic induced by a , the α -characteristic, and postulate the results for the β -characteristic. Note that for fixed $(x_0, y_0) \in \Omega$, two characteristics pass through (x_0, y_0) , i.e., both the α - and β -characteristic. Because the matrix \mathbf{A}^α has rank 2, the rows are linearly dependent and therefore κ_1^α and κ_2^α exist such that

$$\begin{pmatrix} F_r \\ F_s \\ F_t \end{pmatrix} = \kappa_1^\alpha \begin{pmatrix} x_\alpha \\ y_\alpha \\ 0 \end{pmatrix} + \kappa_2^\alpha \begin{pmatrix} 0 \\ x_\alpha \\ y_\alpha \end{pmatrix}. \quad (34)$$

The first row gives $x_\alpha = F_r/\kappa_1^\alpha$. By definition we have $y_\alpha = ax_\alpha$ and hence $y_\alpha = aF_r/\kappa_1^\alpha$. The third row then yields $\kappa_2^\alpha = F_t/y_\alpha = \kappa_1^\alpha F_t/(aF_r)$ which yields $\kappa_2^\alpha = b\kappa_1^\alpha$ by (33). For the sake of brevity we write $\kappa^\alpha = \kappa_1^\alpha$. Then (34) reduces to

$$F_r = \kappa^\alpha x_\alpha, \quad (35a)$$

$$F_s = \kappa^\alpha y_\alpha + b\kappa^\alpha x_\alpha, \quad (35b)$$

$$F_t = b\kappa^\alpha y_\alpha. \quad (35c)$$

The evolution of x, y, u, p and q along the characteristics can be determined from (35),

the strip conditions (6) and (9), respectively, giving

$$x_\alpha = \frac{F_r}{\kappa^\alpha}, \quad (36a)$$

$$y_\alpha = a \frac{F_r}{\kappa^\alpha}, \quad (36b)$$

$$u_\alpha = (p + aq) \frac{F_r}{\kappa^\alpha}, \quad (36c)$$

$$p_\alpha = (r + as) \frac{F_r}{\kappa^\alpha}, \quad (36d)$$

$$q_\alpha = (s + at) \frac{F_r}{\kappa^\alpha}, \quad (36e)$$

where the choice of κ^α determines the parametric scaling of the base curve. The evolution of r, s and t can be obtained using the compatibility conditions (29). To that purpose we rewrite (29) as the underdetermined linear system

$$\begin{pmatrix} F_r y_\alpha & F_t x_\alpha & 0 \\ 0 & F_r y_\alpha & F_t x_\alpha \end{pmatrix} \begin{pmatrix} r_\alpha \\ s_\alpha \\ t_\alpha \end{pmatrix} = -x_\alpha y_\alpha \begin{pmatrix} F^x \\ F^y \end{pmatrix}. \quad (37)$$

By the rank-nullity theorem [15, p. 175] the general solution of (37) reads

$$\begin{pmatrix} r_\alpha \\ s_\alpha \\ t_\alpha \end{pmatrix} = - \begin{pmatrix} \frac{F^x x_\alpha}{F_r} \\ 0 \\ \frac{F^y y_\alpha}{F_t} \end{pmatrix} + \theta^\alpha \begin{pmatrix} \frac{F_t x_\alpha}{F_r y_\alpha} \\ -1 \\ \frac{F_r y_\alpha}{F_t x_\alpha} \end{pmatrix}, \quad (38)$$

where the first terms is the particular solution with $s_\alpha = 0$ and the second terms is an element of the null space of the matrix for arbitrary θ^α . Rewriting this, using (35), yields

$$\begin{pmatrix} r_\alpha \\ s_\alpha \\ t_\alpha \end{pmatrix} = - \frac{1}{\kappa^\alpha} \begin{pmatrix} F^x \\ 0 \\ F^y \end{pmatrix} + \theta^\alpha \begin{pmatrix} b \\ -1 \\ \frac{1}{b} \end{pmatrix}. \quad (39)$$

Because the ODE system (36) depends on a and b , what remains is to determine the evolution of a and b along the characteristics. These are straightforwardly calculated by taking the derivative of (31) w.r.t. α . Treating the β -characteristic analogously to the α -characteristic, we similarly obtain κ^β and θ^β , and the ODE

systems read

$$\begin{aligned}
x_\alpha &= \frac{F_r}{\kappa^\alpha}, & x_\beta &= \frac{F_r}{\kappa^\beta}, \\
y_\alpha &= a \frac{F_r}{\kappa^\alpha}, & y_\beta &= b \frac{F_r}{\kappa^\beta}, \\
u_\alpha &= (p + aq) \frac{F_r}{\kappa^\alpha}, & u_\beta &= (p + bq) \frac{F_r}{\kappa^\beta}, \\
p_\alpha &= (r + as) \frac{F_r}{\kappa^\alpha}, & p_\beta &= (r + bs) \frac{F_r}{\kappa^\beta}, \\
q_\alpha &= (s + at) \frac{F_r}{\kappa^\alpha}, & q_\beta &= (s + bt) \frac{F_r}{\kappa^\beta}, \\
r_\alpha &= \theta^\alpha b - \frac{1}{\kappa^\alpha} F^x, & r_\beta &= \theta^\beta a - \frac{1}{\kappa^\beta} F^x, \\
s_\alpha &= -\theta^\alpha, & s_\beta &= -\theta^\beta, \\
t_\alpha &= \frac{1}{b} \left(\theta^\alpha - \frac{1}{\kappa^\alpha} F^y \right), & t_\beta &= \frac{1}{a} \left(\theta^\beta - \frac{1}{a\kappa^\beta} F^y \right), \\
a_\alpha &= \left(\frac{F_s + \sqrt{\Delta}}{2F_r} \right)_\alpha, & a_\beta &= \left(\frac{F_s + \sqrt{\Delta}}{2F_r} \right)_\beta, \\
b_\alpha &= \left(\frac{F_s - \sqrt{\Delta}}{2F_r} \right)_\alpha, & b_\beta &= \left(\frac{F_s - \sqrt{\Delta}}{2F_r} \right)_\beta,
\end{aligned} \tag{40}$$

where the further evaluation of $a_\alpha, b_\alpha, a_\beta$ and b_β yield no meaningful insight. Note the coupling between the two ODE systems, for example the evolution of r_α depends on b , which forms the direction of the other characteristic via $bx_\beta = y_\beta$. All expressions for the evolution of a and b can be expanded, but neither can be fully expressed in x, y, u and the derivatives of u . Furthermore, as we will see for the Monge-Ampère equation, the evolution for either a or b , does depend both on a and b . Hence, (40) is a mutually coupled system of ODEs.

3 The hyperbolic Monge-Ampère equation

In the remaining of the paper we will consider the hyperbolic Monge-Ampère equation. Recall that the hyperbolic Monge-Ampère equation is given by

$$F(x, y, u, p, q, r, s, t) = rt - s^2 + f^2 = 0 \text{ for } (x, y) \in \Omega, \tag{41}$$

for $\Omega \subseteq \mathbb{R}^2$, the unknown function $u = u(x, y) \in C^3(\Omega)$ and the known function $f = f(x, y) \in C^1(\Omega)$, with $f \neq 0$ on $\bar{\Omega}$. The derivatives of F are

$$F_r = t, \quad F_s = -2s, \quad F_t = r. \tag{42}$$

Furthermore, the characteristic equation is given by

$$D(\mu) = F_r \mu^2 - F_s \mu + F_t = t\mu^2 + 2s\mu + r = 0, \tag{43}$$

and the corresponding discriminant is

$$\Delta = F_s^2 - 4F_r F_t = 4s^2 - 4rt = 4f^2, \tag{44}$$

which is positive, and hence (41) is hyperbolic. The two real and distinct roots of (44) are given by

$$a = \frac{F_s + \sqrt{\Delta}}{2F_r} = \frac{-s + f}{t}, \quad b = \frac{F_s - \sqrt{\Delta}}{2F_r} = \frac{-s - f}{t}. \quad (45)$$

for $t \neq 0$. In case $t = 0$, we express a and b as

$$a = \frac{r}{-s - f}, \quad b = \frac{r}{-s + f}, \quad (46)$$

instead. Furthermore, the auxiliary functions F^x and F^y are given by

$$\begin{aligned} F^x &= F_x + F_u p + F_p r + F_q s = F_x = 2f f_x, \\ F^y &= F_y + F_u q + F_p s + F_q t = F_y = 2f f_y. \end{aligned} \quad (47)$$

From (41) and (45), it follows that

$$a + b = \frac{-2s}{t}, \quad a - b = \frac{2f}{t}, \quad ab = \frac{s^2 - f^2}{t^2} = \frac{r}{t}. \quad (48)$$

From these relations we can express the second derivatives in terms of a, b and f as follows

$$r = \frac{2ab}{a - b} f, \quad s = -\frac{a + b}{a - b} f, \quad t = \frac{2f}{a - b}. \quad (49)$$

The systems of ODEs (40) then read

$$\begin{aligned} x_\alpha &= \frac{t}{\kappa^\alpha}, & x_\beta &= \frac{t}{\kappa^\beta}, \\ y_\alpha &= a \frac{t}{\kappa^\alpha}, & y_\beta &= b \frac{t}{\kappa^\beta}, \\ u_\alpha &= (p + aq) \frac{t}{\kappa^\alpha}, & u_\beta &= (p + bq) \frac{t}{\kappa^\beta}, \\ p_\alpha &= (r + as) \frac{t}{\kappa^\alpha}, & p_\beta &= (r + bs) \frac{t}{\kappa^\beta}, \\ q_\alpha &= (s + at) \frac{t}{\kappa^\alpha}, & q_\beta &= (s + bt) \frac{t}{\kappa^\beta}, \\ r_\alpha &= \theta^\alpha b - \frac{1}{\kappa^\alpha} (f^2)_x, & r_\beta &= \theta^\beta a - \frac{1}{\kappa^\beta} (f^2)_x, \\ s_\alpha &= -\theta^\alpha, & s_\beta &= -\theta^\beta, \\ t_\alpha &= \frac{1}{b} \left(\theta^\alpha - \frac{1}{\kappa^\alpha} (f^2)_y \right), & t_\beta &= \frac{1}{a} \left(\theta^\beta - \frac{1}{\kappa^\beta} (f^2)_y \right). \end{aligned} \quad (50)$$

Note that the ODE systems in (50) contain four parameters, viz. $\kappa^\alpha, \kappa^\beta$, which are determined by an appropriate scaling, and θ^α and θ^β , which are free parameters. Consequently, the derivatives of r, s and t cannot be rewritten such that they no longer depend on θ^α as this would uniquely determine r, s, t along the characteristic strip which contradicts the definition of a characteristic strip. By differentiating the expressions for a and b and using (50) we find the evolution along the α -

characteristic, viz.

$$\begin{aligned} a_\alpha &= \frac{1}{t} \left(1 - \frac{a}{b}\right) \theta^\alpha + \frac{1}{\kappa^\alpha} (f_x + af_y) + \frac{a}{b} \frac{1}{\kappa^\alpha t} (f^2)_y \\ &= \frac{1}{t} \left(1 - \frac{a}{b}\right) \theta^\alpha + \frac{1}{\kappa^\alpha} \left(f_x + \frac{a^2}{b} f_y\right), \end{aligned} \quad (51a)$$

$$\begin{aligned} b_\alpha &= \frac{\theta^\alpha - f_x \frac{t}{\kappa^\alpha} - f_y a \frac{t}{\kappa^\alpha}}{t} - \frac{b}{t} \left(\theta^\alpha - \frac{2ff_y}{\kappa^\alpha}\right) \frac{1}{b} \\ &= -\frac{1}{\kappa^\alpha} (f_x + bf_y). \end{aligned} \quad (51b)$$

The expression for a_α could be rewritten, for example by using (49), but due to $a \neq b$, it will include the unknown θ^α . More fundamentally, we cannot determine a_α explicitly as then both a and b can be uniquely determined along the α -characteristic, from which r, s, t would follow by (49), which contradicts the definition of a characteristic.

Note that we are free to choose κ^α and κ^β due to the freedom in parameterization of the base curve. In the following we conveniently choose $\kappa^\alpha = \kappa^\beta = F_r = t$. Using relations (49) the ODE system (50) reduces to

$$\begin{aligned} x_\alpha &= 1, & x_\beta &= 1, \\ y_\alpha &= a, & y_\beta &= b, \\ u_\alpha &= p + aq, & u_\beta &= p + bq, \\ p_\alpha &= -af, & p_\beta &= bf, \\ q_\alpha &= f, & q_\beta &= -f, \\ r_\alpha &= \theta^\alpha b - (a - b)f_x, & r_\beta &= \theta^\beta a - (a - b)f_x, \\ s_\alpha &= -\theta^\alpha, & s_\beta &= -\theta^\beta, \\ t_\alpha &= \frac{1}{b} (\theta^\alpha - (a - b)f_y), & t_\beta &= \frac{1}{a} (\theta^\beta - (a - b)f_y), \\ a_\alpha &= \frac{a - b}{2f} \left[\left(1 - \frac{a}{b}\right) \theta^\alpha + f_x + \frac{a^2}{b} f_y \right], & a_\beta &= \frac{a - b}{2f} (f_x + af_y), \\ b_\alpha &= \frac{b - a}{2f} (f_x + bf_y), & b_\beta &= -\frac{a - b}{2f} \left[\left(\frac{b}{a} - 1\right) \theta^\beta + f_x + \frac{b^2}{a} f_y \right]. \end{aligned} \quad (52)$$

There is a lot of redundancy in these equations which directly follows from (45), (48) and (49). We therefore reduce (52) by omitting the equations involving θ_α and θ_β . What remains are the ODE systems

$$\begin{aligned} x_\alpha &= 1, & x_\beta &= 1, \\ y_\alpha &= a, & y_\beta &= b, \\ u_\alpha &= p + aq, & u_\beta &= p + bq, \\ p_\alpha &= -af, & p_\beta &= bf, \\ q_\alpha &= f, & q_\beta &= -f, \\ b_\alpha &= \frac{b - a}{2f} (f_x + bf_y), & a_\beta &= \frac{a - b}{2f} (f_x + af_y), \end{aligned} \quad (53)$$

which we integrate numerically. Recall that: “every strip, which has one point in common with the integral surface and all its tangent planes equal to that of

the integral surface, lies entirely on said surface.”, which furthermore justifies the reduction of (52) to (53), as only u, p, q and the characteristics, so u, p, q, a and b , need to be known.

3.1 Boundary conditions

We solve (41) on a rectangular domain $\Omega = [x_{\min}, x_{\max}] \times [y_{\min}, y_{\max}]$, for $x_{\min}, x_{\max}, y_{\min}, y_{\max} \in \mathbb{R}$, with $x_{\min} < x_{\max}, y_{\min} < y_{\max}$ and we call $\{x_{\min}\} \times [y_{\min}, y_{\max}]$ the initial base curve. We extend the initial base curve to an initial C_1 -strip by supplementing it with $u_W, p_W : [y_{\min}, y_{\max}] \rightarrow \mathbb{R}$, where we prescribe $u(x_{\min}, y) = u_W(y)$ and $p(x_{\min}, y) = p_W(y)$ for some u_W, p_W . The subscript ‘W’ is used as the values are prescribed on the Western part of $\partial\Omega$, see Figure 5.

If the initial strip is a free strip, then prescribing u_W, p_W uniquely determines the C_2 -strip as an extension of the initial base curve. To verify this, we check whether the characteristic condition (30) holds. Therefore we parameterize the initial base curve as $x(\lambda) = 0, y(\lambda) = \lambda, \lambda \in [0, 1]$, then $x_\lambda = 0, y_\lambda = 1$ and the characteristic condition yields $ty_\lambda^2 + 2sx_\lambda y_\lambda + rx_\lambda^2 = t = 0$. Hence if $t \neq 0$ on the initial strip, i.e., if $u''_W(y) \neq 0$, the initial strip is a free strip. Henceforth we assume $u''_W(y) \neq 0$, which then implies the initial base curve uniquely extends to a C_2 -strip, and we can uniquely determine q, a, b, r, s, t on the initial strip via

$$q(x_{\min}, y) = u'_W(y), \quad (54a)$$

$$t(x_{\min}, y) = u''_W(y), \quad (54b)$$

$$s(x_{\min}, y) = p'_W(y), \quad (54c)$$

$$a(x_{\min}, y) = \frac{-s(x_{\min}, y) + f_W(y)}{t(x_{\min}, y)}, \quad (54d)$$

$$b(x_{\min}, y) = \frac{-s(x_{\min}, y) - f_W(y)}{t(x_{\min}, y)}, \quad (54e)$$

$$r(x_{\min}, y) = \frac{2a(x_{\min}, y)b(x_{\min}, y)}{a(x_{\min}, y) - b(x_{\min}, y)} f_W(y), \quad (54f)$$

where $f_W(y) := f(x_{\min}, y)$. For the lower and upper boundary, i.e., for $y \in \{y_{\min}, y_{\max}\}$, the required boundary conditions are more delicate. To understand this let $\mathbf{x}_\alpha = (x_\alpha, y_\alpha)$ and $\mathbf{x}_\beta = (x_\beta, y_\beta)$ denote the tangent vectors of the characteristics. Let $\mathbf{b} \in \partial\Omega$ and $\hat{\mathbf{n}}$ the outward unit normal vector on the boundary. We classify the α -characteristics, and similarly the β -characteristic, based on whether they are entering or leaving the domain as follows

- Leaving characteristic if $\mathbf{x}_\alpha(\mathbf{b}) \cdot \hat{\mathbf{n}} > 0$,
- Entering characteristic if $\mathbf{x}_\alpha(\mathbf{b}) \cdot \hat{\mathbf{n}} < 0$,
- Boundary characteristic if $\mathbf{x}_\alpha(\mathbf{b}) \cdot \hat{\mathbf{n}} = 0$,

which is schematically shown in Figure 4 for $y = y_{\min}$.

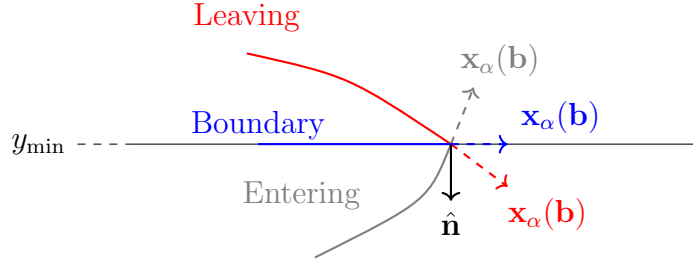


Figure 4: Schematic classification of characteristics.

We assume $a(x, y)$ and $b(x, y)$ to be well defined for all $(x, y) \in \Omega$ and the Monge-Ampère equation to be hyperbolic, which implies there are two characteristics passing through each point $(x, y) \in \Omega$. By classifying the characteristics as entering or leaving, one can determine if and how many additional boundary conditions need to be prescribed at each boundary point. Boundary characteristics should be treated as leaving characteristics. We distinguish three cases: one characteristic entering, two characteristics entering and zero characteristics entering in the point \mathbf{b} on the boundary.

Case 1. One characteristic leaving and one entering the domain, either

$$\mathbf{x}_\alpha \cdot \hat{\mathbf{n}} > 0, \mathbf{x}_\beta \cdot \hat{\mathbf{n}} < 0 \quad \text{or} \quad \mathbf{x}_\alpha \cdot \hat{\mathbf{n}} < 0, \mathbf{x}_\beta \cdot \hat{\mathbf{n}} > 0. \quad (55)$$

An example of this case is shown in Figure 5 at $y = y_{\min}$, with N, W, S, E denoting the Western, Northern, Southern and Eastern boundary segments of the domain. The curves denote one α - (dashed) and one β -characteristic (dotted). At \mathbf{b} , the values u, p, q and b can be computed from the ODE system for the α -characteristic. However, a cannot be determined because the evolution of a along the α -characteristic is unknown. Therefore we should impose one boundary condition, which is the initial condition for the entering β -characteristic, such that a can be computed. We can either prescribe a directly, or prescribe either r, s or t and compute a from inverting (49), viz.

$$a = \frac{br}{r - 2bf}, \quad a = \frac{s - f}{s + f}b, \quad a = b + \frac{2f}{t} \quad (56)$$

The remaining two unknowns of r, s and t then follow from (49).

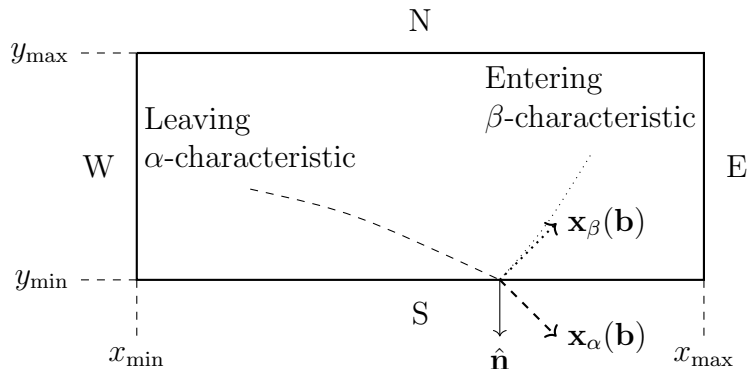


Figure 5: Schematic overview of a rectangular domain where the α -characteristic leaves, and the β -characteristic enters the domain.

Case 2. Two characteristics entering the domain, i.e.,

$$\mathbf{x}_\alpha \cdot \hat{\mathbf{n}} < 0, \quad \mathbf{x}_\beta \cdot \hat{\mathbf{n}} < 0. \quad (57)$$

In this situation the values of u, p, q, a and b cannot be determined (see Figure 6). Therefore we prescribe u and its derivative normal to the line segment, which is q if the line segment is horizontal (as in Figure 6), or p if it is vertical. The calculation of the relevant variables at $y = y_{\min}$ and $y = y_{\max}$ follow analogously to (54). As example we consider the line segment at $y = y_{\min}$. Let $u_S, q_S : [x_{\min}, x_{\max}] \rightarrow \mathbb{R}$ be given and let $u(x, y_{\min}) = u_S(x)$ and $q(x, y_{\min}) = q_S(x)$. We obtain u, p, a, b, r, s and t at $y = y_b$ via

$$p(x, y_{\min}) = u'_S(x), \quad (58a)$$

$$r(x, y_{\min}) = u''_S(x), \quad (58b)$$

$$s(x, y_{\min}) = q'_S(x), \quad (58c)$$

$$a(x, y_{\min}) = -\frac{r(x, y_{\min})}{s(x, y_{\min}) + f_S(x)}, \quad (58d)$$

$$b(x, y_{\min}) = -\frac{r(x, y_{\min})}{s(x, y_{\min}) - f_S(x)}, \quad (58e)$$

$$t(x, y_{\min}) = \frac{2f_S(x)}{a(x, y_{\min}) - b(x, y_{\min})}. \quad (58f)$$

We require $u''_S(x) \neq 0$ in this case, such that the hyperbolicity condition $a(x, y_b) \neq b(x, y_b)$ is satisfied. Note that the initial strip is one example of *Case 2*, where two characteristics enter. To see this, note that

$$\begin{aligned} \mathbf{x}_\alpha \cdot \hat{\mathbf{n}} &= -x_\alpha = -1 < 0, \\ \mathbf{x}_\beta \cdot \hat{\mathbf{n}} &= -x_\beta = -1 < 0, \end{aligned} \quad (59)$$

thus classifying both as entering characteristics.

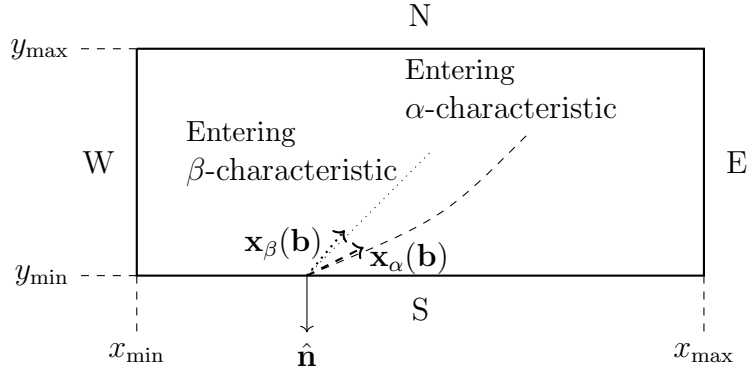


Figure 6: Schematic overview of a rectangular domain where both an α - and β -characteristic enter the domain at $y = y_{\min}$.

Case 3. Two characteristic leaving the domain, i.e.,

$$\mathbf{x}_\alpha \cdot \hat{\mathbf{n}} > 0, \quad \mathbf{x}_\beta \cdot \hat{\mathbf{n}} > 0. \quad (60)$$

Here, we should not prescribe anything at all as all values are known, or can be determined by integrating the ODE systems of the α - and β -characteristics, see Figure 7. Note that this situation is identical to that of an interior point.

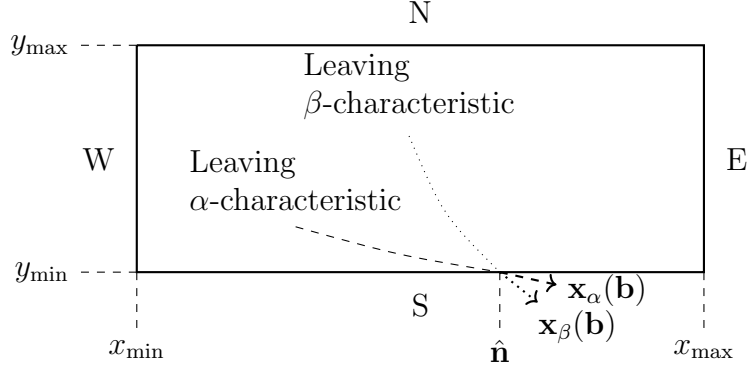


Figure 7: Schematic overview of a rectangular domain where both an α - and β -characteristic leave the domain $y = y_{\min}$.

Note that at $x = x_{\max}$, $x_{\alpha} = 1$ and $x_{\beta} = 1$ such that $\mathbf{x}_{\alpha} \cdot \hat{\mathbf{n}} > 0$ and $\mathbf{x}_{\beta} \cdot \hat{\mathbf{n}} > 0$, hence this boundary segment coincides with Case 3. The possible exception being the corner points (x_{\max}, y_{\min}) and (x_{\max}, y_{\max}) because the normal is not uniquely defined. In this case the point should be treated as in the Cases 1 or 2. Classifying the boundary segment $x = x_{\max}$ as Case 3 is a direct consequence of choice $\kappa^{\alpha} = \kappa^{\beta} = t$, such that $x_{\alpha} = 1$ and $x_{\beta} = 1$ for the two characteristic families.

4 Numerical methods

In order to solve (53) we rewrite it as

$$\frac{d\mathbf{v}^{\alpha}}{d\alpha} = \mathbf{g}^{\alpha}(\mathbf{v}^{\alpha}, a), \quad \frac{d\mathbf{v}^{\beta}}{d\beta} = \mathbf{g}^{\beta}(\mathbf{v}^{\beta}, b), \quad (61a)$$

$$\mathbf{v}^{\alpha} = \begin{pmatrix} x \\ y \\ u \\ p \\ q \\ b \end{pmatrix}, \quad \mathbf{v}^{\beta} = \begin{pmatrix} x \\ y \\ u \\ p \\ q \\ a \end{pmatrix}, \quad \mathbf{g}^{\alpha} = \begin{pmatrix} 1 \\ a \\ p + aq \\ -af \\ f \\ \frac{b-a}{2f}(f_x + bf_y) \end{pmatrix}, \quad \mathbf{g}^{\beta} = \begin{pmatrix} 1 \\ b \\ p + bq \\ bf \\ -f \\ \frac{a-b}{2f}(f_x + af_y) \end{pmatrix}. \quad (61b)$$

Equations (61) are two mutually coupled systems because the evolution of a and b are determined on the other characteristic. By supplying initial conditions, the problem can be treated as a Cauchy problem which we solve by numerical integration.

For our numerical grid we choose N_x points in the x -direction and N_y in the y -direction. Let the grid points $\mathbf{x}_{i,j}$ be given by $\mathbf{x}_{i,j} = (x_i, y_j)$ for $i = 1, \dots, N_x, j = 1, \dots, N_y$. We choose the grid to be equidistant in the y -direction with spacing $h_y = (y_{\max} - y_{\min}) / (N_y - 1)$. The grid spacing in the x -direction does not need to be equidistant, i.e., we write $(h_x)_i = x_{i+1} - x_i$. This adaptive stepsize will be

detailed in Section 4.4. We denote the numerical approximation of u in a grid point as $u_{i,j} \approx u(\mathbf{x}_{i,j})$, and likewise for the other variables.

When discussing numerical methods we generally consider one step at a time, i.e., we consider the evolution from the grid line $x = x_i$ to the line $x = x_{i+1}$. Therefore it is convenient to write $h_x = (h_x)_i$ when no ambiguity arises.

4.1 Numerical method based on forward Euler

In this section we will introduce a numerical scheme based on the forward Euler method to calculate $\mathbf{v}_{i+1,j}^\alpha$ and $\mathbf{v}_{i+1,j}^\beta$ given $\mathbf{v}_{i,j}^\alpha$ and $\mathbf{v}_{i,j}^\beta$.

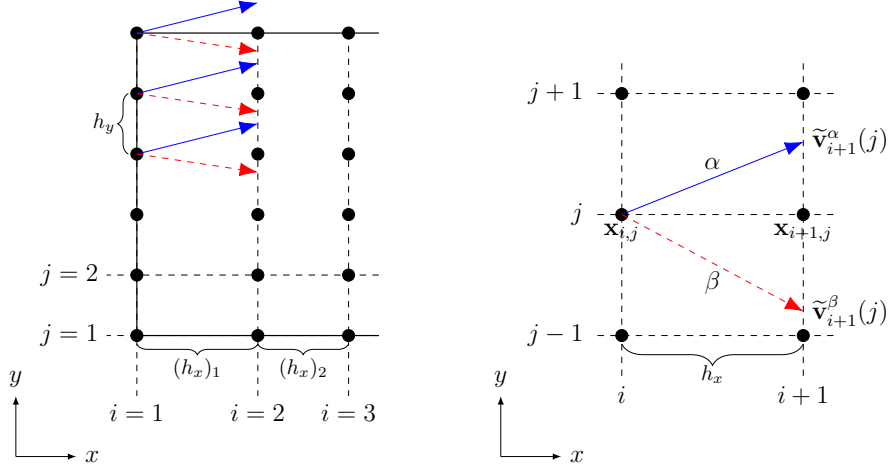


Figure 8: Schematic representation of the numerical method using forward Euler.

The numerical stencil is schematically shown in Figure 8. The black dots represent the grid points. The solid blue and dashed red arrows correspond to the numerical approximation of the α - and β characteristic, respectively. At the grid points these characteristics are approximated using forward Euler, i.e., we approximate the characteristics as tangent lines passing through grid points $\mathbf{x}_{i,j}$ and having slope $a_{i,j}$ for the α -characteristic and $b_{i,j}$ for the β -characteristic. This implies that for a step size h_x , the two characteristics departing from $\mathbf{x}_{i,j}$ arrive at $(x_{i+1}, \tilde{y}_{i+1}^\alpha(j))$ and $(x_{i+1}, \tilde{y}_{i+1}^\beta(j))$ for the α - and β -characteristic respectively, where

$$x_{i+1} = x_i + h_x, \quad (62a)$$

$$\tilde{y}_{i+1}^\alpha(j) = y_j + h_x a_{i,j}, \quad (62b)$$

$$\tilde{y}_{i+1}^\beta(j) = y_j + h_x b_{i,j}. \quad (62c)$$

The points $(x_{i+1}, \tilde{y}_{i+1}^\alpha(j))$ and $(x_{i+1}, \tilde{y}_{i+1}^\beta(j))$ do generally not coincide with any gridpoint. Similarly we can calculate u, p, q on both characteristics, while a and b can only be determined on one characteristic. More compactly written, we have the following forward Euler step:

$$\tilde{\mathbf{v}}_{i+1}^\alpha(j) = \mathbf{v}_{i,j}^\alpha + h_x \mathbf{g}^\alpha(\mathbf{v}_{i,j}^\alpha, a_{i,j}), \quad \tilde{\mathbf{v}}_{i+1}^\beta(j) = \mathbf{v}_{i,j}^\beta + h_x \mathbf{g}^\beta(\mathbf{v}_{i,j}^\beta, b_{i,j}). \quad (63)$$

Here $\tilde{\mathbf{v}}_{i+1}^\alpha(j)$ denotes the new values of \mathbf{v}^α at $(x_{i+1}, \tilde{y}_{i+1}^\alpha(j))$ for which the corresponding characteristic passes through the grid point $\mathbf{x}_{i,j}$ as shown in Figure 8.

Analogously we define $\tilde{\mathbf{v}}_{i+1}^\beta(j)$. Because we are interested in obtaining $\mathbf{v}^\alpha(x_{i+1}, y_j)$ and $\mathbf{v}^\beta(x_{i+1}, y_j)$, we interpolate $\tilde{\mathbf{v}}_{i+1}^\alpha(j)$ and $\tilde{\mathbf{v}}_{i+1}^\beta(j)$. Let the y, u, p, q -components of $\tilde{\mathbf{v}}_{i+1}^\alpha(j)$ be denoted by $\tilde{y}_{i+1}^\alpha(j), \tilde{u}_{i+1}^\alpha(j), \tilde{p}_{i+1}^\alpha(j)$ and $\tilde{q}_{i+1}^\alpha(j)$, respectively, and similarly for $\tilde{\mathbf{v}}_{i+1}^\beta(j)$. Two approaches to carry out the interpolation are shown in Figure 9, using linear interpolation.

Approach 1: We consider all values computed for each characteristic family, e.g. $\tilde{u}_{i+1}^\alpha(j)$, as one set and interpolate using local B-Splines ([16, p. 90-97]; see App. 4.1) within that set, which yields the approximations $u_{i+1,j}^\alpha$ and $u_{i+1,j}^\beta$. Because we have no a priori preference whether $u_{i+1,j}^\alpha$ or $u_{i+1,j}^\beta$ approximates $u_{i+1,j}$ better, we average the results and set

$$u_{i+1,j} = \frac{u_{i+1,j}^\alpha + u_{i+1,j}^\beta}{2}. \quad (64)$$

Similarly we obtain $p_{i+1,j}$ and $q_{i+1,j}$.

Approach 2: We collect $\tilde{u}_{i+1}^\alpha(j)$ and $\tilde{u}_{i+1}^\beta(j)$ for all $j = 1, \dots, N_y$ in one set and interpolate using local B-Splines over that set to obtain $u_{i+1,j}$. Similarly we obtain $p_{i+1,j}$ and $q_{i+1,j}$.

Numerical results show that neither of these methods outperforms the other significantly or consistently. Computationally both approaches are approximately equally expensive [17]. Approach 1 will be used throughout.

Various subtleties arise using the approach above. For one, a and b are known along one family of characteristics only, so we use one set of values for interpolation of these variables. In the case a grid point is not located between two numerically estimated characteristics, which may occur for a grid point on the boundary, then we supplement the missing boundary value as detailed in Section 3.1.

To determine an appropriate spline interpolant we consider both the error associated with one forward Euler step and that of the interpolation. The local truncation error of the forward Euler method is $\mathcal{O}(h_x^2)$ [18, p. 335]. In Section 4.4 we introduce a method to control the step size h_x , which consequently implies that the local truncation error behaves as $\mathcal{O}(h_y^2)$. The error of a spline interpolant of order n , also called a spline interpolant of degree $n - 1$, is $\mathcal{O}(h_y^n)$ [16, p. 95]. In general we choose the degree of the spline interpolant such that its order matches the order of the integration method. For the forward Euler method this implies a spline interpolant of order 2 which is standard local linear interpolation.

4.2 Numerical method based on modified Euler

In this section we will discuss a numerical scheme based on the modified Euler scheme. The local truncation error of the modified Euler method is $\mathcal{O}(h_x^3)$.

First we calculate a predictor by doing a forward Euler step of step size $\frac{h_x}{2}$ for (61), viz.

$$\tilde{\mathbf{v}}_{i+\frac{1}{2}}^\alpha(j) = \mathbf{v}_{i,j}^\alpha + \frac{h_x}{2} \mathbf{g}^\alpha(\mathbf{v}_{i,j}^\alpha, a_{i,j}), \quad \tilde{\mathbf{v}}_{i+\frac{1}{2}}^\beta(j) = \mathbf{v}_{i,j}^\beta + \frac{h_x}{2} \mathbf{g}^\beta(\mathbf{v}_{i,j}^\beta, b_{i,j}). \quad (65)$$

We adhere to the same notation as in the previous section, where a tilde denotes the function value on the corresponding characteristic which is not necessarily located at a grid point.

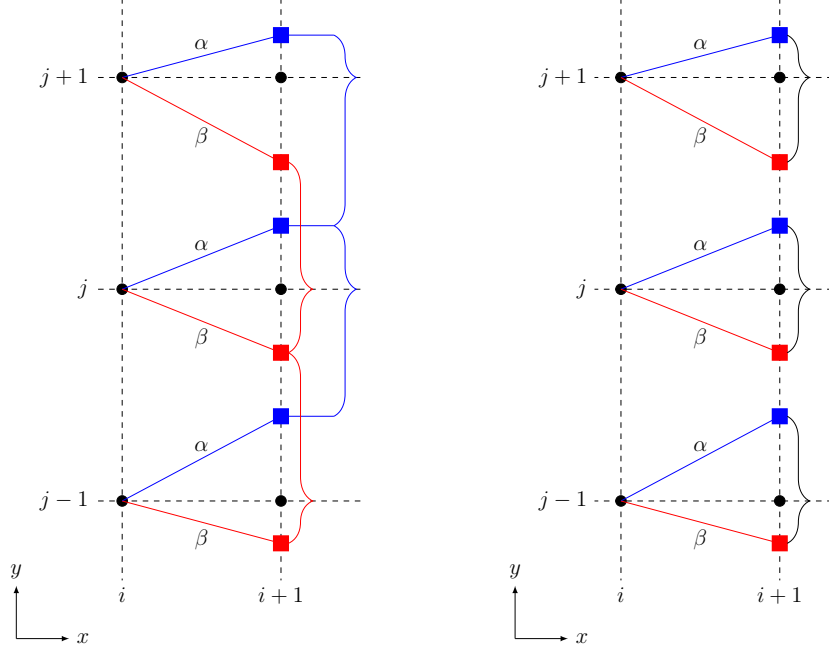


Figure 9: Schematic representation of linear interpolation where a curly bracket denotes the values used for interpolation and the gridpoint it influences. Interpolation for u , p and q can be done either using two distinct sets, formed by the two characteristic families (Approach 1, left), or using both sets combined (Approach 2, right).

Because a and b are not known but are needed at $x_{i+1/2}$ along the α - and β -characteristic, respectively, we approximate them using interpolation. We interpolate the a -component of $\tilde{\mathbf{v}}_{i+1/2}^\beta(j)$, known at the points $\tilde{y}_{i+1/2}^\beta(j)$ to the points $\tilde{y}_{i+1/2}^\alpha(j)$, which approximate $a(x_{i+1/2}, \tilde{y}_{i+1/2}^\alpha(j))$. We denote this approximation by $a_{i+1/2,j}$. In the same way we approximate $b_{i+1/2,j}$ from $\tilde{\mathbf{v}}_{i+1/2}^\alpha(j)$. The modified Euler step is then given by

$$\tilde{\mathbf{v}}_{i+1}^\alpha(j) = \mathbf{v}_{i,j}^\alpha + h_x \mathbf{g}^\alpha(\tilde{\mathbf{v}}_{i+1/2}^\alpha(j), a_{i+1/2,j}), \quad \tilde{\mathbf{v}}_{i+1}^\beta(j) = \mathbf{v}_{i,j}^\beta + h_x \mathbf{g}^\beta(\tilde{\mathbf{v}}_{i+1/2}^\beta(j), b_{i+1/2,j}). \quad (66)$$

We conclude the modified Euler step by interpolating to the grid points using Approach 1, as discussed in Section 4.1. We choose third order spline interpolation for the modified Euler method, as it corresponds to its local truncation error.

4.3 Numerical method based on classic Runge-Kutta

In this section we will introduce the classic Runge-Kutta method. Following a similar approach, we can generalize our integration methods to other higher order explicit Runge-Kutta methods.

First we make a forward Euler step of size $\frac{h_x}{2}$ for (61) viz.

$$\tilde{\mathbf{v}}_{i+1/2}^\alpha(j) = \mathbf{v}_{i,j}^\alpha + \frac{h_x}{2} \mathbf{g}^\alpha(\mathbf{v}_{i,j}^\alpha, a_{i,j}), \quad \tilde{\mathbf{v}}_{i+1/2}^\beta(j) = \mathbf{v}_{i,j}^\beta + \frac{h_x}{2} \mathbf{g}^\beta(\mathbf{v}_{i,j}^\beta, b_{i,j}). \quad (67)$$

As in the case of the modified Euler based method, we interpolate the a - and b -components of $\tilde{\mathbf{v}}_{i+\frac{1}{2}}^\beta(j)$ and $\tilde{\mathbf{v}}_{i+\frac{1}{2}}^\alpha(j)$ to approximate $a_{i+\frac{1}{2},j}$ and $b_{i+\frac{1}{2},j}$, respectively. Second, we do a step of size $\frac{h_x}{2}$ with the slope based on the previously found values of $\tilde{\mathbf{v}}^\alpha$ and $\tilde{\mathbf{v}}^\beta$, viz.

$$\hat{\mathbf{v}}_{i+\frac{1}{2}}^\alpha(j) = \mathbf{v}_{i,j}^\alpha + \frac{h_x}{2} \mathbf{g}^\alpha(\tilde{\mathbf{v}}_{i+\frac{1}{2}}^\alpha(j), a_{i+\frac{1}{2},j}), \quad \hat{\mathbf{v}}_{i+\frac{1}{2}}^\beta(j) = \mathbf{v}_{i,j}^\beta + \frac{h_x}{2} \mathbf{g}^\beta(\tilde{\mathbf{v}}_{i+\frac{1}{2}}^\beta(j), b_{i+\frac{1}{2},j}), \quad (68)$$

where we used a hat to distinguish between the different stages. Similar as before we interpolate a and b from the β - and α -characteristics to the α - and β -characteristics to obtain $\hat{a}_{i+\frac{1}{2},j}$ and $\hat{b}_{i+\frac{1}{2},j}$, respectively. Using these slopes we do a step of size h_x which yields

$$\hat{\mathbf{v}}_{i+1}^\alpha(j) = \mathbf{v}_{i,j}^\alpha + h_x \mathbf{g}^\alpha(\hat{\mathbf{v}}_{i+\frac{1}{2}}^\alpha(j), \hat{a}_{i+\frac{1}{2},j}), \quad \hat{\mathbf{v}}_{i+1}^\beta(j) = \mathbf{v}_{i,j}^\beta + h_x \mathbf{g}^\beta(\hat{\mathbf{v}}_{i+\frac{1}{2}}^\beta(j), \hat{b}_{i+\frac{1}{2},j}). \quad (69)$$

Interpolating the a - and b -components of $\hat{\mathbf{v}}_{i+1}^\beta(j)$ and $\hat{\mathbf{v}}_{i+1}^\alpha(j)$ yields approximations for $\hat{a}_{i+1}^\alpha(j)$ and $\hat{b}_{i+1}^\beta(j)$, respectively. Finally the full Runge-Kutta step is given by

$$\tilde{\mathbf{v}}_{i+1}^\alpha(j) = \mathbf{v}_{i,j}^\alpha + \frac{h_x}{6} \left(\mathbf{g}^\alpha(\mathbf{v}_{i,j}^\alpha, a_{i,j}) + 2\mathbf{g}^\alpha(\tilde{\mathbf{v}}_{i+\frac{1}{2}}^\alpha(j), a_{i+\frac{1}{2},j}) + 2\mathbf{g}^\alpha(\hat{\mathbf{v}}_{i+\frac{1}{2}}^\alpha(j), \hat{a}_{i+\frac{1}{2},j}) + \mathbf{g}^\alpha(\hat{\mathbf{v}}_{i+1}^\alpha(j), \hat{a}_{i+1}^\alpha(j)) \right), \quad (70a)$$

$$\tilde{\mathbf{v}}_{i+1}^\beta(j) = \mathbf{v}_{i,j}^\beta + \frac{h_x}{6} \left(\mathbf{g}^\beta(\mathbf{v}_{i,j}^\beta, b_{i,j}) + 2\mathbf{g}^\beta(\tilde{\mathbf{v}}_{i+\frac{1}{2}}^\beta(j), b_{i+\frac{1}{2},j}) + 2\mathbf{g}^\beta(\hat{\mathbf{v}}_{i+\frac{1}{2}}^\beta(j), \hat{b}_{i+\frac{1}{2},j}) + \mathbf{g}^\beta(\hat{\mathbf{v}}_{i+1}^\beta(j), \hat{b}_{i+1}^\beta(j)) \right). \quad (70b)$$

We conclude the Runge-Kutta step by interpolating $\tilde{\mathbf{v}}_{i+1}^\alpha(j)$ and $\tilde{\mathbf{v}}_{i+1}^\beta(j)$ using fifth order spline interpolation to the grid points using Approach 1, as discussed in Section 4.1.

4.4 Dynamic step size control

In this section we introduce a procedure to choose the step size h_x adaptively. We aim to reduce the computational error while maintaining convergence, which depends both on the integration method and the interpolation methods.

Because integration is done in the positive x -direction, the corresponding discretization error is a function of h_x . On the other hand, we interpolate in the y -direction, but the interpolation error is not solely a function of h_y as we will see. Ideally we want both the integration and interpolation error to be of the same order, such that neither of them dominates. Asymptotically, this is obtained most easily by using both an integration and interpolation method of the same order, and choosing the discretization steps in the x - and y -direction of the same order of magnitude as well. In the x -direction the discretization step size is h_x , though the distance between the interpolation nodes, those points that are the intersection between a grid line and the numerical approximation of the characteristics, is not equidistant, but rather follows from both the evolution along the characteristics (53) and the integration method used. Without loss of generality, we solely consider the

β -characteristic. Let $\Delta y(j) = |\tilde{y}_{i+1}^\beta(j) - y_j|$ denote the distance between, on the one hand, the intersection point of (the approximation of) the β -characteristic at $x = x_{i+1}$, and on the other hand, the point (x_{i+1}, y_j) , as shown in Figure 10 for $j = 1$. Approximating $\Delta y(j)$ by a forward Euler step yields

$$\Delta y(j) = |y_j + (h_x)_i b_{i,j} - y_j| = |b_{i,j}|(h_x)_i. \quad (71)$$

Hence $\Delta y(j) \leq h_y$ is obtained if we choose

$$(h_x)_i < h_y \min_{j \in \{1, \dots, N_y\}} (1, 1/|b_{i,j}|), \quad (72)$$

where the constant “1” is chosen such that $(h_x)_i < h_y$, regardless of the slope of the characteristics. This allows us to control the error of the numerical methods by solely controlling h_y . Similarly we would like to have $(h_x)_i < h_y \min(1, 1/|a_{i,j}|)$ for all $j = 1, \dots, N_y$. Therefore we choose

$$(h_x)_i = \gamma h_y \cdot \min_{j \in \{1, \dots, N_y\}} \left\{ 1, \left| \frac{1}{a_{i,j}} \right|, \left| \frac{1}{b_{i,j}} \right| \right\}, \quad (73)$$

where $0 \leq \gamma \leq 1$ is a tuning parameter. Generally we choose $\gamma = 0.95$, as this implies strict inequality.

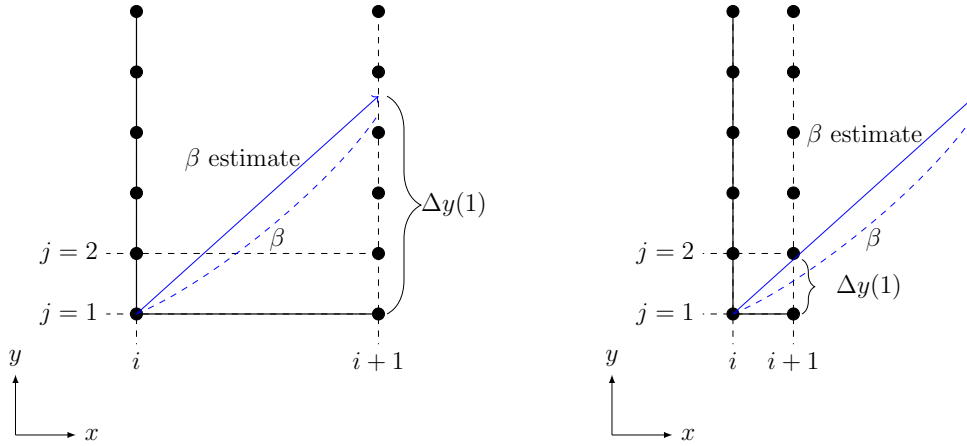


Figure 10: Two schematic situations of Δy , as function of $(h_x)_i$.

4.5 Residual of the Monge-Ampère equation

We solve the mutually coupled ODE systems (53) without calculating r , s or t nor by calculating any numerical derivatives. Ideally we should be able to determine the numerical residual without numerically taking derivatives either. We do so by formulating the Monge-Ampère equation as an integral equation, which we evaluate numerically.

The Monge-Ampère equation can be written as $p_x q_y - p_y q_x + f^2 = 0$, which only depends on f^2 and the derivatives of p and q . We can rewrite it in terms of ∇p and ∇q . To this end let \mathbf{J} be the symplectic matrix $\begin{pmatrix} 0 & 1 \\ -1 & 0 \end{pmatrix}$, from which the two equivalent formulations

$$-f^2 = \nabla \cdot (p \mathbf{J} \nabla q), \quad (74a)$$

$$f^2 = \nabla \cdot (q \mathbf{J} \nabla p), \quad (74b)$$

follow, where we used $\nabla \cdot (\mathbf{J}\nabla\phi) = 0$ for a scalar function ϕ , and $\nabla \cdot (\phi\mathbf{P}) = \phi\nabla \cdot \mathbf{P} + \mathbf{P} \cdot \nabla\phi$ with \mathbf{P} a vector-valued function. Let $A \subseteq \Omega$ be an orientable domain and let $\hat{\mathbf{n}}$ be the outward unit normal on ∂A . By subsequently integrating the right-hand side of (74a) over A and applying Gauss's theorem we obtain

$$\iint_A \nabla \cdot (p\mathbf{J}\nabla q) \, dA = \oint_{\partial A} p\mathbf{J}\nabla q \cdot \hat{\mathbf{n}} \, ds = \oint_{\partial A} p\nabla q \cdot \hat{\boldsymbol{\tau}} \, ds, \quad (75)$$

where we defined $\hat{\boldsymbol{\tau}} = \mathbf{J}^T \hat{\mathbf{n}}$. Note that $\hat{\boldsymbol{\tau}}$ is the unit tangent vector to the domain taken in the counter clockwise direction. It follows from (74) that

$$\iint_A f^2 \, dA = - \oint_{\partial A} p\nabla q \cdot \hat{\boldsymbol{\tau}} \, ds, \quad (76a)$$

and in a similar way we find:

$$\iint_A f^2 \, dA = \oint_{\partial A} q\nabla p \cdot \hat{\boldsymbol{\tau}} \, ds. \quad (76b)$$

Note that adding these equations yields

$$\oint_{\partial A} (p\nabla q + q\nabla p) \cdot \hat{\boldsymbol{\tau}} \, ds = 0, \quad (77)$$

which trivially holds by Stokes' theorem since $p\nabla q + q\nabla p = \nabla(pq)$ is conservative. Because the integral formulations (76) are both equivalent to the Monge-Ampère equation, we use numerical approximations of (76) as a measure for the residual of the numerical solution. To this purpose, let

$$\mathbf{H}_1 = -p\nabla q = -p \begin{pmatrix} s \\ t \end{pmatrix} = \frac{pf}{a-b} \begin{pmatrix} a+b \\ -2 \end{pmatrix}, \quad (78a)$$

$$\mathbf{H}_2 = q\nabla p = q \begin{pmatrix} r \\ s \end{pmatrix} = \frac{qf}{a-b} \begin{pmatrix} 2ab \\ -a-b \end{pmatrix}. \quad (78b)$$

Equations (76) are equivalent to

$$\iint_A f^2 \, dA = \oint_{\partial A} \mathbf{H}_k \cdot \hat{\boldsymbol{\tau}} \, ds, \quad (79)$$

for $k = 1, 2$. Choosing an appropriate domain A , this can therefore be used to determine the numerical residual. We choose the control volume $A = A_{i,j} = [x_{i-\frac{1}{2}}, x_{i+\frac{1}{2}}] \times [y_{j-\frac{1}{2}}, y_{j+\frac{1}{2}}]$, and write (79) as

$$I_k^N + I_k^S + I_k^W + I_k^E - \iint_{A_{i,j}} f^2 \, dA = 0, \quad (80)$$

where

$$\begin{aligned} I_k^N &= - \int_{x_{i-\frac{1}{2}}}^{x_{i+\frac{1}{2}}} H_{k,x}(x, y_{j+\frac{1}{2}}) \, dx, & I_k^S &= \int_{x_{i-\frac{1}{2}}}^{x_{i+\frac{1}{2}}} H_{k,x}(x, y_{j-\frac{1}{2}}) \, dx, \\ I_k^W &= - \int_{y_{j-\frac{1}{2}}}^{y_{j+\frac{1}{2}}} H_{k,y}(x_{i-\frac{1}{2}}, y) \, dy, & I_k^E &= \int_{y_{j-\frac{1}{2}}}^{y_{j+\frac{1}{2}}} H_{k,y}(x_{i+\frac{1}{2}}, y) \, dy, \end{aligned} \quad (81)$$

and $H_{k,x}$ denotes the x -component of \mathbf{H}_k , and the line integrals are carried out over the North, South, West and East part of the control volume $A_{i,j}$, as shown in Figure 11.

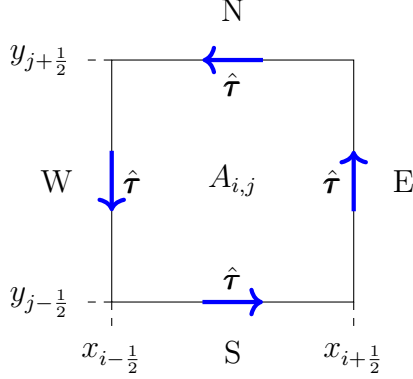


Figure 11: Schematic overview of domain $A_{i,j}$ with corresponding tangent vectors.

We approximate the integrals I_k^N , I_k^S , I_k^W and I_k^E using Gauss-Legendre quadrature rules. To this end, let $z_1, z_2 \in \mathbb{R}$, $z_1 < z_2$ and $g \in C([z_1, z_2])$. Given the n points ξ_i and n weights w_i (see [19] for example), we approximate

$$\int_{z_1}^{z_2} g(x) dx \approx \frac{z_2 - z_1}{2} \sum_{i=1}^n w_i g\left(\frac{z_2 - z_1}{2} \xi_i + \frac{z_1 + z_2}{2}\right). \quad (82)$$

In case g is $2n$ times continuously differentiable, the error associated with (82) is $\mathcal{O}((z_2 - z_1)^{2n+1})$ [20, §5.2]. Therefore, we choose $n = 3$ such that the calculation of the residual is asymptotically more accurate than the integration methods used for stepping from one grid line to the next. Note that we generally do not know \mathbf{H}_k in the points $(\frac{z_2 - z_1}{2} \xi_i + \frac{z_1 + z_2}{2})$, where either $(z_1, z_2) = (x_{i-1/2}, x_{i+1/2})$ or $(z_1, z_2) = (y_{i-1/2}, y_{i+1/2})$. Therefore, we interpolate \mathbf{H}_k using splines of order 5, such that the interpolation is at least as accurate as the step method. Similarly, we approximate $\iint_{A_{i,j}} f^2 dA$ by subsequently integrating over x and y using the Gauss-Legendre quadrature rule. We normalize the absolute residual of (80) over $A_{i,j}$ by dividing it by the area $|A_{i,j}|$, and denote the result by $\epsilon_k(i, j)$. Lastly, we measure the residual over the whole grid by

$$\epsilon_k = \max_{\substack{i \in \{2, \dots, N_x - 1\} \\ j \in \{2, \dots, N_y - 1\}}} \epsilon_k(i, j). \quad (83)$$

5 Numerical results

In this section we present numerical results for the Monge-Ampère equation. We will present results for the forward Euler, modified Euler and classic Runge-Kutta based methods for a default test case (Section 5.1), an example of which the analytical solution is known. For the modified Euler method we furthermore consider 2nd, 3rd and 5th order splines. In Section 5.2, we compare the methods for a different neat example. Additionally, we show numerical results for the Runge-Kutta

based method, for which we prescribe either two or zero boundary conditions per boundary segment (Section 5.3), a case where the number of boundary conditions varies along the boundary (Section 5.4) and a case where one boundary value is nonsmooth (Section 5.5).

5.1 Default test case

To validate the numerical methods we design a default test case. To this end we let $\Omega = [0, 1] \times [-0.5, 0.5]$ and we calculate a right-hand side-solution pair (f, u) using the method outlined in App. B with $w(z) = \cos(iz)$, giving

$$\begin{aligned} u(x, y) &= \cos(y) \cosh(x), \\ f(x, y) &= \sqrt{\frac{\cos(2y) + \cosh(2x)}{2}}. \end{aligned} \quad (84)$$

From the exact solution (84) and (45) we find a and b on the whole domain, viz.

$$a(x, y) = -\frac{\sin(y) \sinh(x) + f(x, y)}{\cos(y) \cosh(x)}, \quad (85a)$$

$$b(x, y) = \frac{-\sin(y) \sinh(x) + f(x, y)}{\cos(y) \cosh(x)}. \quad (85b)$$

We impose the corresponding initial conditions

$$u(0, y) = \cos(y), \quad p(0, y) = 0. \quad (86)$$

By (54) we find

$$\begin{aligned} q(0, y) &= -\sin(y), & t(0, y) &= -\cos(y), & s(0, y) &= 0, \\ a(0, y) &= -1, & b(0, y) &= 1, & r(0, y) &= \cos(y). \end{aligned} \quad (87)$$

To justify (86), note that the outward unit normal vector $\hat{\mathbf{n}}$ on the initial strip is $\hat{\mathbf{n}}(0, y) = (-1, 0)^\top$, $\mathbf{x}_\alpha(0, y) = (1, -1)^\top$ and $\mathbf{x}_\beta(0, y) = (1, 1)^\top$. Therefore $\mathbf{x}_\alpha(0, y) \cdot \hat{\mathbf{n}}(0, y) = \mathbf{x}_\beta(0, y) \cdot \hat{\mathbf{n}}(0, y) = -1$, and hence we should prescribe u and p on the initial strip according to Case 2 in Section 3.1. A similar calculations show that at $x = 1$ no boundary conditions need to be prescribed. On the upper boundary, we have $\hat{\mathbf{n}} = (0, 1)^\top$, $\mathbf{x}_\alpha = (1, a)^\top$, $\mathbf{x}_\beta = (1, b)^\top$, $a < 0$ and $b > 0$, so that the α -characteristic is entering the domain. Hence we need to prescribe b and a is known. In the same way, we need to prescribe a at the lower boundary and b is known.

5.1.1 Forward Euler based method

We present the results for the forward Euler based method for which we use splines of first degree, i.e., linear interpolants. The convergence of the forward Euler scheme is shown in Figure 12 as function of h_y , which controls $(h_x)_i$; see Section 4.4. In the left figure the maximum absolute differences at $x = 1$ between the function value and its numerical approximation for several variables are shown. More precisely, the figure shows

$$E[a] := \max_{j=1, \dots, N_y} \frac{1}{N_y} |a(x_{N_x}, y_j) - a_{N_x, j}|, \quad (88)$$

and similar errors for b, u, p and q for varying h_y . The dynamic step size control implies $(h_x)_i \approx \mathcal{O}(h_y)$, which allows us to quantify the error solely in terms of h_y .

It is well known that the forward Euler method is locally second order accurate and globally first order, if the solutions are sufficiently smooth. Because the interpolation error and the local discretization error are both second order accurate, we expect the global convergence to be that of the forward Euler method, i.e., first order, which is also seen in the figure.

The residuals are also shown and show first order convergence for ϵ_1 , ϵ_2 defined by (83). To understand this, note that as we divide by the area of the control volume, that is we divide by $|A_{i,j}|$, by which we effectively normalize ϵ_1 , ϵ_2 such that they converge as the integrand does, which in this case is first order (for \mathbf{H}_1 and \mathbf{H}_2).

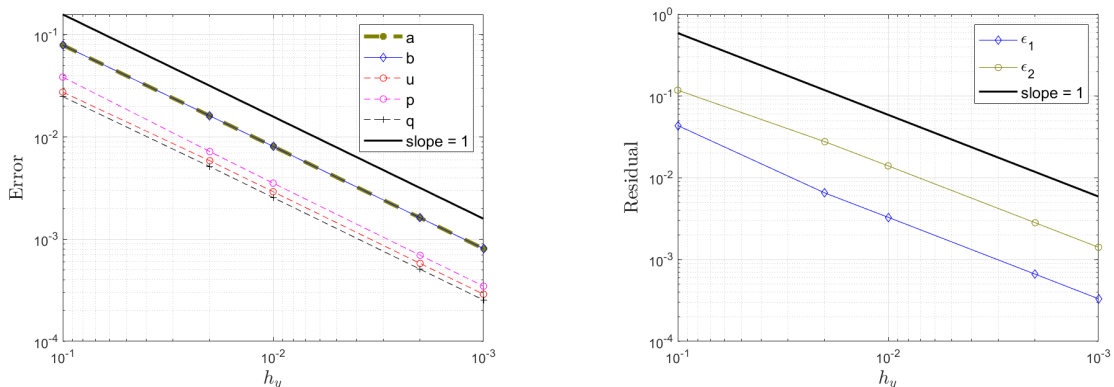


Figure 12: Convergence of the global error (left) and the residual (right) for the forward Euler based method.

Figure 13 shows both the solution surface u (left), and a color map of the residual ϵ_1 for the case $N_y = 1000$. The surface u clearly is both smooth and a saddle surface. The right image shows the residual along with some characteristics. The shown characteristics are calculated after the simulation is done, and chosen such that they enter at 7 equidistant points on the initial strip and 5 on the upper and lower boundary. The direction of the characteristics clearly shows that both the blue characteristic, i.e., the α -characteristic, and the black characteristic, i.e., the β -characteristic, enter at the initial strip. Hence, both u and p need to be prescribed at the initial strip. This is in agreement with (86). Furthermore, it shows that the α -characteristics and β -characteristics leave the domain at the lower and upper boundary, respectively. Therefore a and b should be prescribed at the lower and upper boundary, respectively, agrees with the discussion on boundary conditions above.

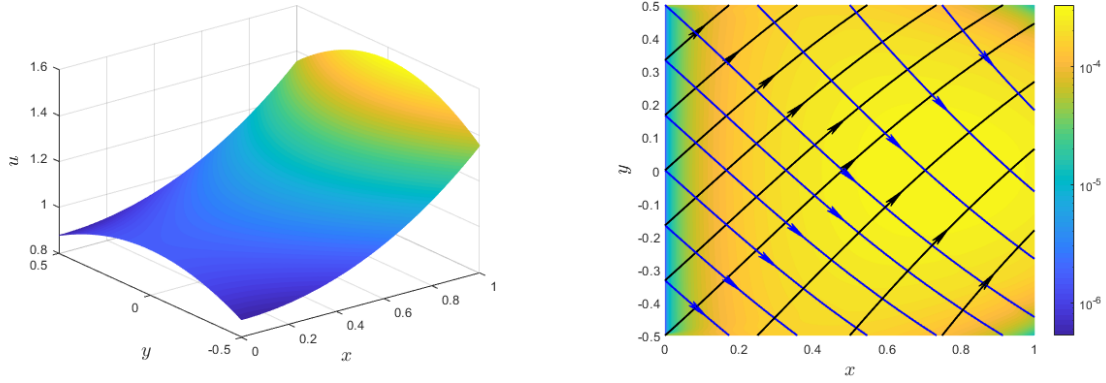


Figure 13: Surface u (left) and a color map of the residual ϵ_1 with characteristics (right).

5.1.2 Modified Euler based method

In this section we will discuss a few results for the modified Euler based method. We demonstrate the importance of choosing an appropriate interpolation routine and show accompanying convergence results. Generally we use an interpolant which is as accurate as the integration routine because a more accurate interpolant will not increase the overall accuracy while being computationally more expensive, and a lower order interpolant will lower the convergence. In Figures 14, 15 and 16 the convergence is shown for splines of order 2, 3, and 5, respectively. Using splines of second order yields first order convergence for both the global error and the residual. This is in agreement with the expectation due to the local discretization error after interpolation being second order. Henceforth, second order splines, i.e., linear B-splines, reduce the rate of convergence, and higher order splines are preferred.

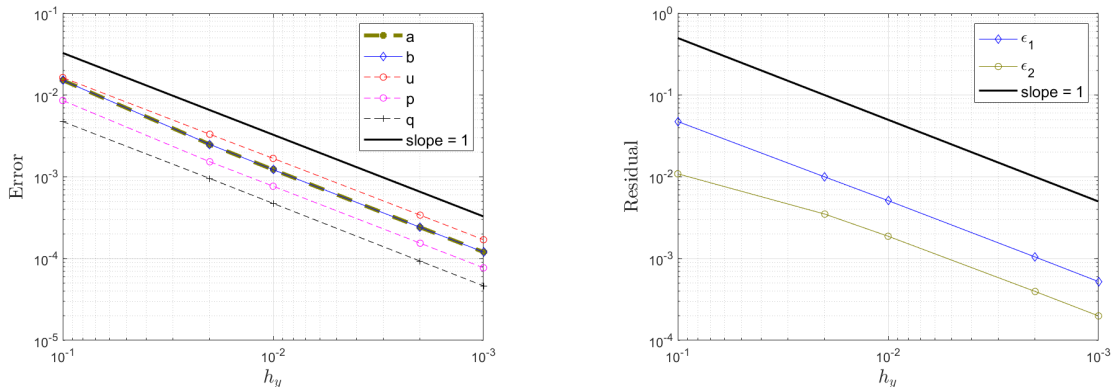


Figure 14: Convergence for the global error (left) and the residual (right) for the modified Euler based method with a second order accurate interpolant.

Figures 15 and 16 show the same order of convergence because the interpolants are at least as accurate as the local integration error. For a spline of order 3, i.e., quadratic B-splines, the interpolation error is as accurate as the local error of the modified Euler method. The accuracy of the global error is one order lower and equal to that of the residual. For the spline of order 5, i.e., for polynomials

of fourth degree as B-splines, the local error of the modified Euler method is the limiting factor and the global error and the residual are second order accurate.

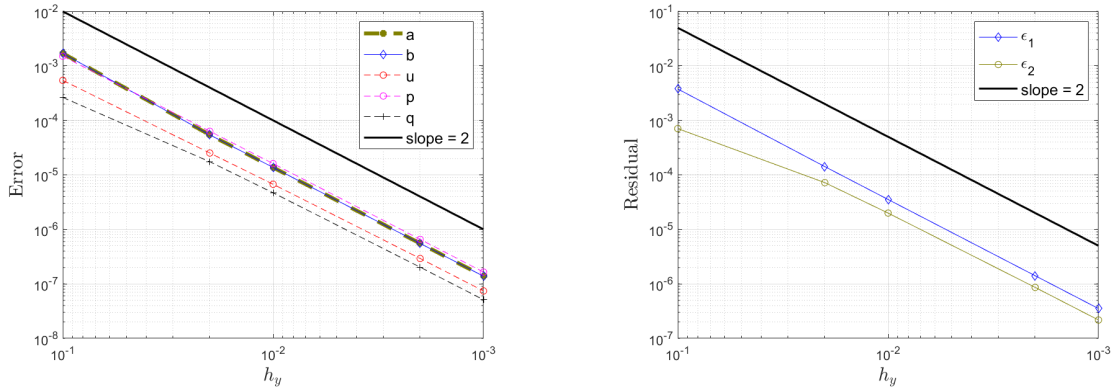


Figure 15: Convergence for the global error (left) and the residual (right) for the modified Euler based method with a third order accurate interpolant.

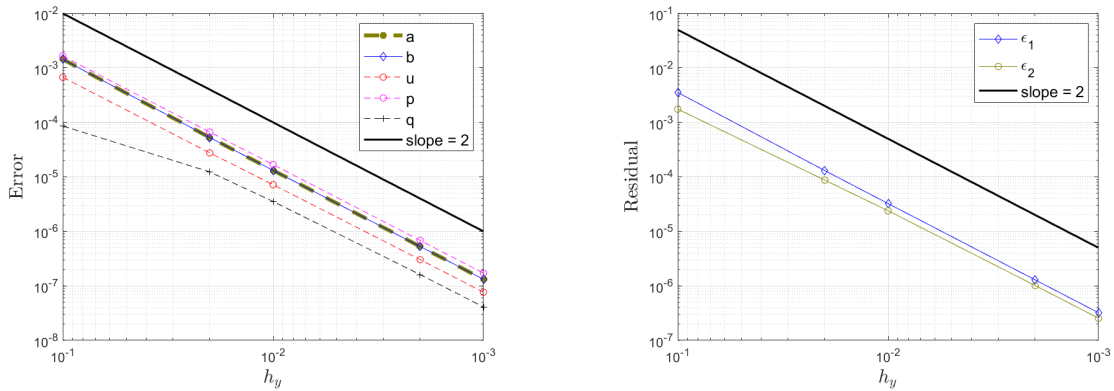


Figure 16: Convergence for the global error (left) and the residual (right) for the modified Euler based method with a fifth order accurate interpolant.

5.1.3 Classic Runge-Kutta based method

Analogously to the previous sections, we consider the default test case. Figure 17 shows the results for using the Runge-Kutta method with spline interpolants of order 5. Because the Runge-Kutta method is locally fifth order accurate, which coincides with the accuracy of the splines, we expect a fourth order global convergence. This is indeed shown in the figure. The convergence of the residuals is also expected to be of order 4, as also seen in the figure. The convergence seems to slow down for $h_y \approx 1/1000$, which is due to round-off errors as the solutions reaches the used computer precision.

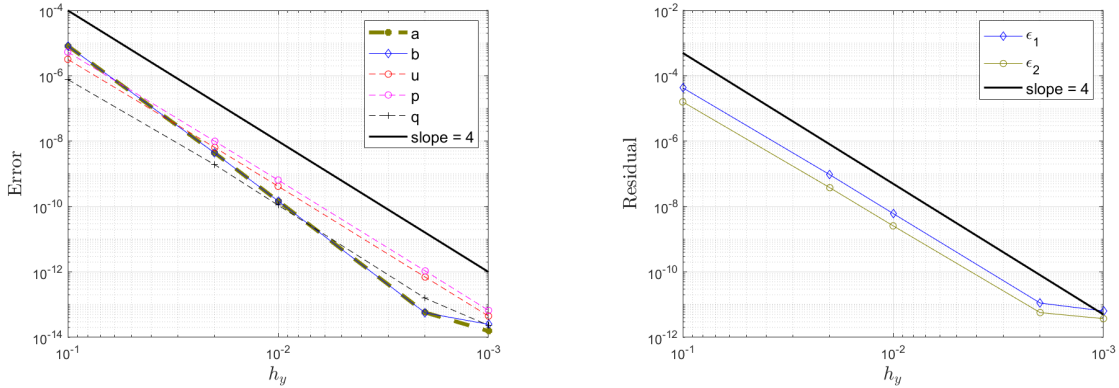


Figure 17: Convergence for the global error (left) and the residual (right) for the classic Runge-Kutta based method with a fifth order accurate interpolant.

5.2 An aggregated example

Next we compare the developed numerical methods for the example

$$u(x, y) = e^x \cos(y), \quad f(x, y) = e^x, \quad (89)$$

which is constructed using $w(z) = e^z$; see App. B. Let $\Omega = [0, 2] \times [-1/3, 2/3]$ be the computational domain. A straightforward calculation using (89) shows

$$\begin{aligned} p(x, y) &= e^x \cos(y), & q(x, y) &= -e^x \sin(y) \\ a(x, y) &= -\frac{\sin(y) + 1}{\cos(y)}, & b(x, y) &= \frac{-\sin(y) + 1}{\cos(y)}, \end{aligned} \quad (90)$$

which we use, along with (89), to prescribe u, p, q, a, b on the initial strip $x = 0$, $-\frac{1}{3} \leq y \leq \frac{2}{3}$, accordingly. Equations (90) show $a < 0$, $b > 0$ on Ω . Analogously to the default test case, we prescribe a on the lower and b on the upper boundary as dictated by (90). We compare the forward Euler, modified Euler and Runge-Kutta methods using second, third and fifth order splines, respectively. The results are shown in Figure 18. The left figure shows first, second and fourth order convergence of the global error of $u_{i,j}$ for the forward Euler, modified Euler and Runge-Kutta-method, respectively. These rates of convergence are in agreement with the previous sections. The convergence of ϵ_1 , shown in the right figure, also shows first, second and fourth order convergence. Furthermore, the convergence of the global error and residual stagnates for the Runge-Kutta-method at $h_y \approx 10^{-3}$. Figure 19 shows that the error accumulates for increasing x , i.e., the further in the domain, as measured from the initial strip, the higher the error. Due to the error being of computer precision near $x = 0$ for $h_y = 10^{-3}$, this accumulation of errors bounds the global error $E[u]$ from below. Closed form bounds for $E[u]$ are not known, though it is evident that it depends on the computational domain and the boundary conditions prescribed.

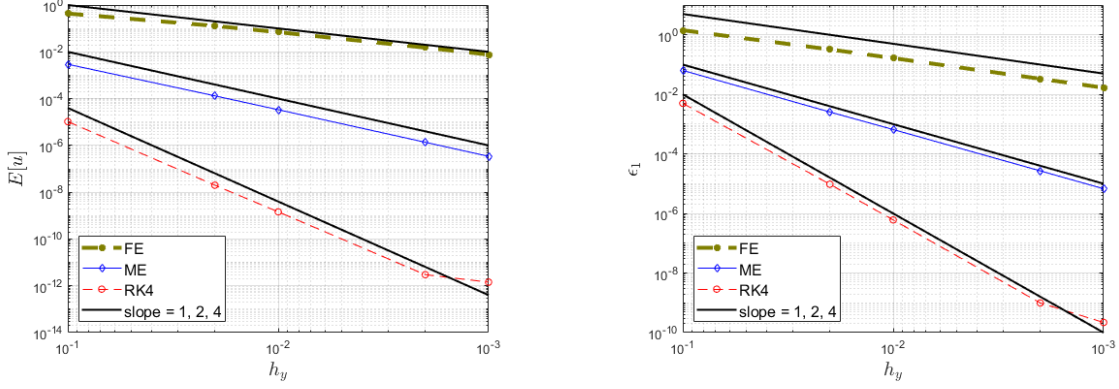


Figure 18: Convergence for the global error (left) and the residual (right).

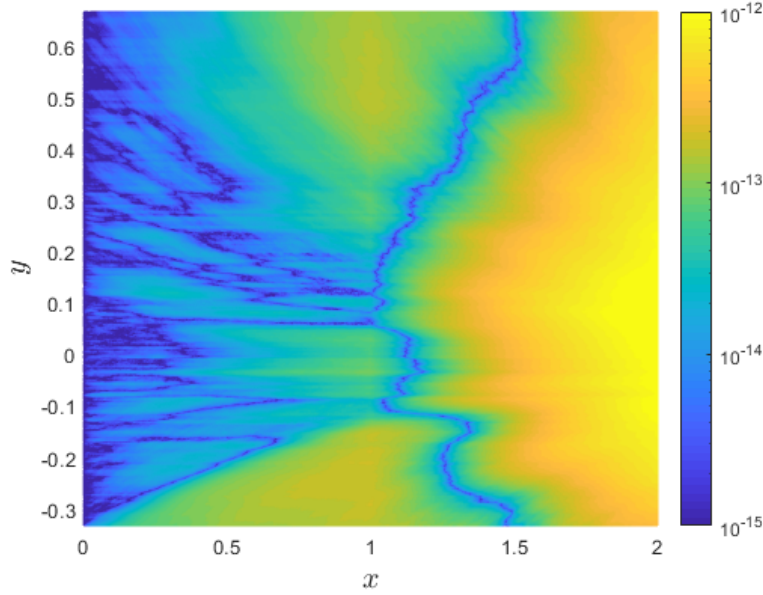


Figure 19: The error $|u_{i,j} - u(\mathbf{x}_{i,j})|$ over the domain for $h_y = 10^{-3}$.

5.3 An initial strip extended over two edges

We will demonstrate an example for the forward Euler based method for which we have two entering characteristics at both the Western and Northern boundary, and two leaving characteristics on both the Southern and Eastern boundary. In this case the Northern boundary is also an initial strip as discussed in Section 3.1. To this end let

$$u(x, y) = x^3 y^2 + 1, \quad f(x, y) = 2\sqrt{6}x^2 y, \quad (91)$$

on the domain $\Omega = [1, 2]^2$. A straightforward calculation shows that (91) satisfies the Monge-Ampère equation (41), and that

$$a(x, y) = \frac{(-3 + \sqrt{6})y}{x}, \quad b(x, y) = -\frac{(3 + \sqrt{6})y}{x}, \quad (92)$$

which implies $a, b < 0$ on Ω . Let $\hat{\mathbf{n}}_W$ denote the normal at the Western boundary segment, and likewise for the other subscripts. It follows that

$$\begin{aligned}
\mathbf{x}_\alpha(1, y) \cdot \hat{\mathbf{n}}_W &< 0, & \mathbf{x}_\beta(1, y) \cdot \hat{\mathbf{n}}_W &< 0, \\
\mathbf{x}_\alpha(x, 1) \cdot \hat{\mathbf{n}}_S &> 0, & \mathbf{x}_\beta(x, 1) \cdot \hat{\mathbf{n}}_S &> 0, \\
\mathbf{x}_\alpha(2, y) \cdot \hat{\mathbf{n}}_N &> 0, & \mathbf{x}_\beta(2, y) \cdot \hat{\mathbf{n}}_N &> 0, \\
\mathbf{x}_\alpha(x, 2) \cdot \hat{\mathbf{n}}_E &< 0, & \mathbf{x}_\beta(x, 2) \cdot \hat{\mathbf{n}}_E &< 0.
\end{aligned} \tag{93}$$

The classification of the boundary conditions in Section 3.1, imply we should prescribe two boundary conditions at the Western and Northern boundaries and zero boundary conditions at the Eastern and Southern segments. By prescribing two boundary conditions to the Northern boundary, it is an initial strip. The total set of prescribed boundary conditions thus read

$$u(1, y) = y^2 + 1, \quad p(1, y) = 3y^2, \quad u(x, 2) = 4x^3 + 1, \quad q(x, 2) = 4x^3. \tag{94}$$

From $u(1, y)$ and $p(1, y)$ we obtain q, r, s, t, a, b at the Western boundary by (54). Analogously, $u(x, 2)$ and $q(x, 2)$ determine p, a, b, r, s, t at the northern boundary.

Figure 20 shows some characteristics for this example, which nicely demonstrates where characteristics are entering or leaving the domain. Furthermore, the figure shows that Ω is fully covered by the domain of dependence of the two initial strips. The figure on the right also shows the points $(1.7, 1.6)$ and $(1.1, 1.1)$ with their corresponding domain of dependence colored red.

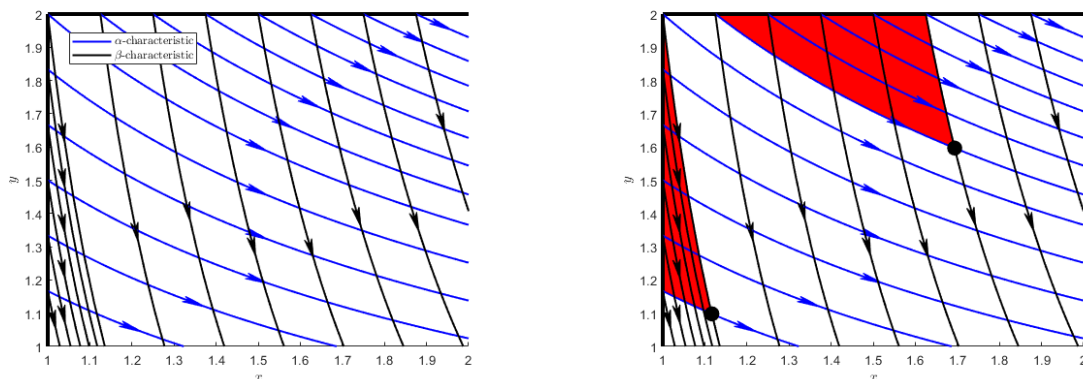


Figure 20: Domain Ω and some characteristics, which enter the domain at the Western and Northern boundaries, with the domain of dependence for the points $(1.7, 1.6)$ and $(1.1, 1.1)$.

Figure 21 shows the convergence for the Euler based method for this example, for both the global error and the residual. As expected, both show first order convergence. Figure 22 shows the error in b for this example, calculated using the Runge-Kutta method with fifth order splines with $h_y = 1/1000$. The figure shows the accumulation of numerical errors over the domain and shows b is most accurate near the boundaries where both a and b are prescribed.

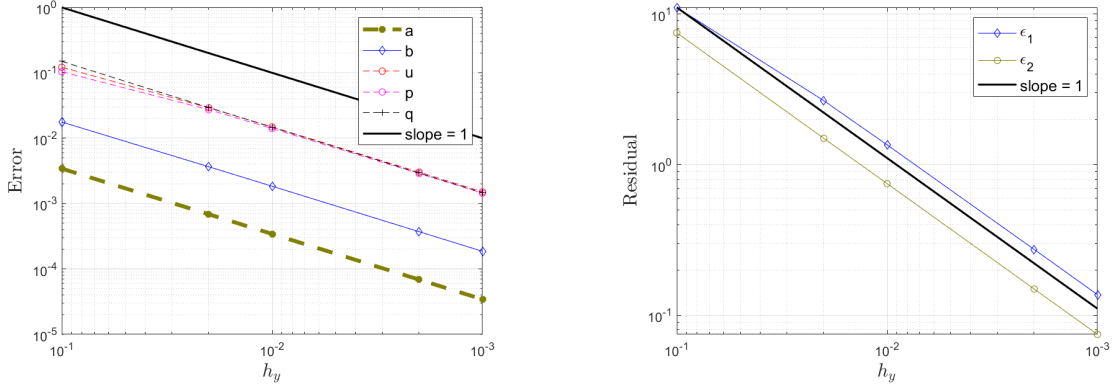


Figure 21: Convergence for the global error (left) and the residual (right) for the forward Euler based method with a second order accurate interpolant.

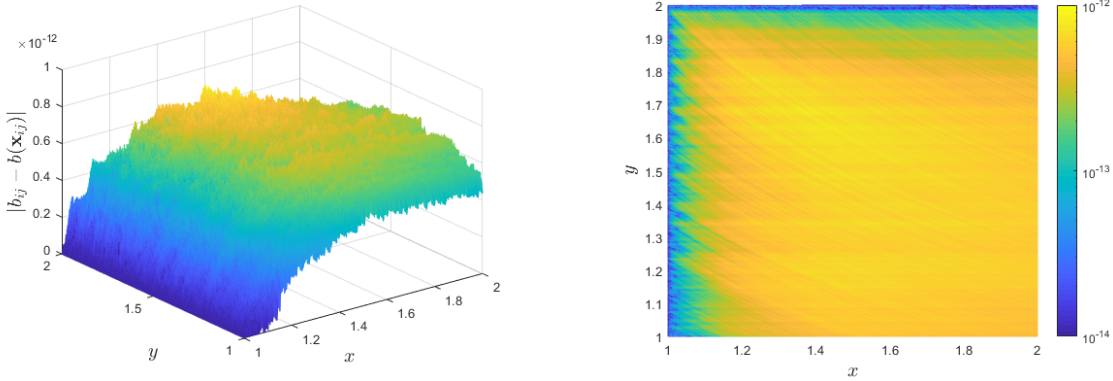


Figure 22: The numerical error $|b_{i,j} - b(\mathbf{x}_{i,j})|$.

5.4 Varying number of boundary conditions

Next we will show an example for which the number of boundary conditions we prescribe changes along the boundary. To this end let $\Omega = [1, 2.5] \times [-2, -1.5]$ and

$$u(x, y) = 1 + e^{2y/x}, \quad f(x, y) = \frac{2}{x^2} e^{2y/x}. \quad (95)$$

It follows that

$$a(x, y) = 1 + \frac{y}{x}, \quad b(x, y) = \frac{y}{x}, \quad (96)$$

which implies $a \leq 0$ for $x \geq -y$, $a > 0$ for $x < -y$ and $b < 0$ on Ω . Let $\hat{\mathbf{n}}$ be the outward unit normal, then the boundary conditions to be prescribed are

Boundary segment	Classification	Boundary condition(s)
Western,	$(\mathbf{x}_\alpha, \hat{\mathbf{n}}) < 0$, $(\mathbf{x}_\beta, \hat{\mathbf{n}}) < 0$,	a and b ,
Southern, left,	$(\mathbf{x}_\alpha, \hat{\mathbf{n}}) > 0$, $(\mathbf{x}_\beta, \hat{\mathbf{n}}) > 0$,	None,
Southern, right,	$(\mathbf{x}_\alpha, \hat{\mathbf{n}}) < 0$, $(\mathbf{x}_\beta, \hat{\mathbf{n}}) > 0$,	b ,
Northern, left,	$(\mathbf{x}_\alpha, \hat{\mathbf{n}}) < 0$, $(\mathbf{x}_\beta, \hat{\mathbf{n}}) < 0$,	a and b ,
Northern, right,	$(\mathbf{x}_\alpha, \hat{\mathbf{n}}) > 0$, $(\mathbf{x}_\beta, \hat{\mathbf{n}}) < 0$,	a ,
Eastern,	$(\mathbf{x}_\alpha, \hat{\mathbf{n}}) > 0$, $(\mathbf{x}_\beta, \hat{\mathbf{n}}) > 0$,	None,

as illustrated in Figure 23.

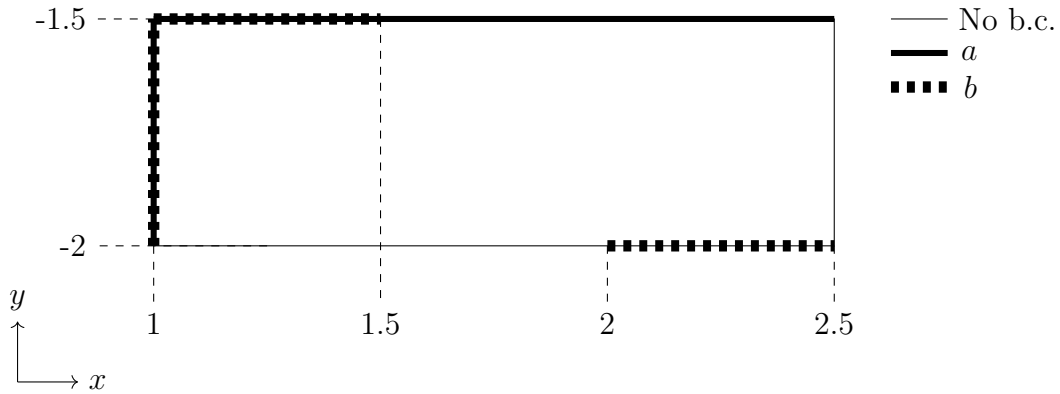


Figure 23: Schematic overview of the prescribed boundary conditions and their locations.

Figure 24 shows the convergence of the global error and the residual for the Runge-Kutta based method with fifth order splines. The convergence is fourth order as expected, and slowly comes to a halt for a fine grid, as also discussed in the previous section. Figure 25 shows the characteristics in the domain (left), and a heatmap of the error $|b_{i,j} - b(\mathbf{x}_{i,j})|$ (right). The heatmap clearly shows the swirling influence of the α -characteristics, and a lower error near the segments of the boundary where b is prescribed.

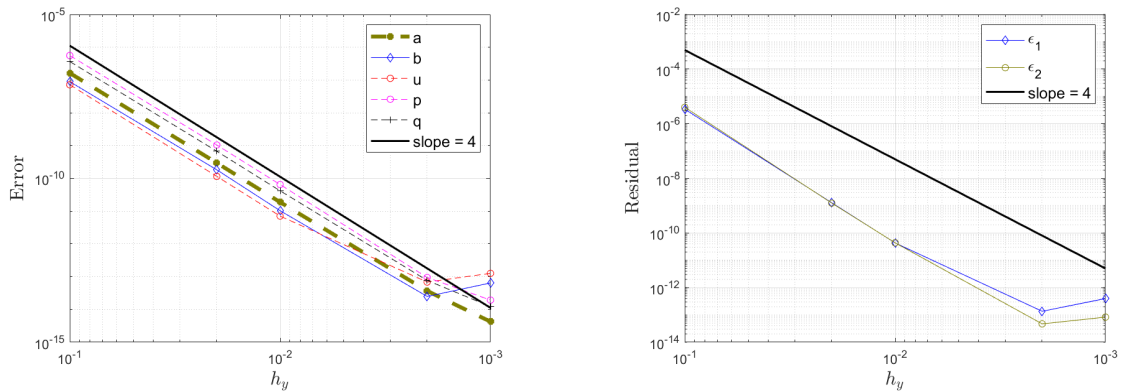


Figure 24: Convergence of the global error (left) and the residual (right).

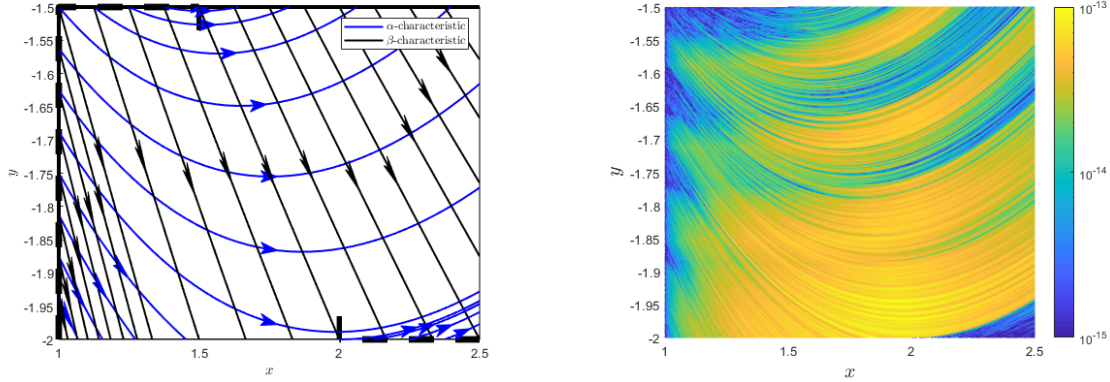


Figure 25: Characteristics in the domain (left) and a heatmap of the numerical error in b (right).

5.5 A problem with nonsmooth boundary conditions

The last example is similar to the default test case of Section 5.1, but now with nonsmooth boundary conditions. As before, we set $\Omega = [0, 1] \times [-0.5, 0.5]$. The initial conditions are the same as before, given by (84) and (86). At the lower and upper boundary, we now use

$$a(x, -0.5) = -e^{-3x/2}(x^2 + 1), \quad (97a)$$

$$b(x, 0.5) = \frac{-\sin(0.5) \sinh(x) + f(x, 0.5)}{\cos(0.5) \cosh(x)}, \quad (97b)$$

respectively, where purposely $a(x, -0.5)$ as given by 97, does not correspond to a of the default test case, (85a). The prescribed b is continuous and smooth while the prescribed a is continuous but nonsmooth at the point $(0, -0.5)$, i.e.,

$$\left. \frac{db(x, 0.5)}{dx} \right|_{x=0} = \left. \frac{db(0, y)}{dy} \right|_{y=-0.5}, \quad (98)$$

$$\left. \frac{da(x, -0.5)}{dx} \right|_{x=0} \neq \left. \frac{da(0, y)}{dy} \right|_{y=-0.5}. \quad (99)$$

The latter statement can be established by applying the identities

$$a_x = \frac{-s_x + f_x}{t} - \frac{-s + f}{t^2} t_x = \frac{-s_x + f_x - at_x}{t}, \quad s_x = r_y, \quad t_x = s_y, \quad (100)$$

to the initial strip (87) to obtain $a_x(0, -0.5) \approx 0.546$, while the derivative of a as given by (97) is $a_x(0, -0.5) \approx -0.878$. Hence a is nonsmooth. Generally the error terms of our numerical methods depend on derivatives of the functions to be estimated. As a is nonsmooth, we do not necessarily expect convergence as we did before. Furthermore, no analytical solution is known for this particular example, therefore we base convergence on the residual values.

We use the Runge-Kutta method with fifth order splines for this example. Figure 26 shows the convergence of the residual (left), and a heat map of ϵ_1 , i.e., the magnitude of the residual on a color scale, in the right figure. The heat map, and surface plots in this section, are constructed for $N_y = 1001$. The figure shows convergence of the solution, although at a slower rate than for continuous boundary

values. The heat map also shows a few characteristics given by the solid white and dashed yellow curves. Furthermore, it shows that the discontinuity of the derivatives of a in $(0, -0.5)$ yields a locally distinct residual. This difference in residual is propagated along the characteristic starting in $(0, -0.5)$. This coincides with an alternative equivalent definition of a characteristic, from [14, p. 408]: “Discontinuities (of a nature to be specified later) of a solution cannot occur except along characteristics.”. We add to this that the discontinuities mentioned, only arise in the second order derivatives, and u, p and q are smooth as seen in Figure 27. The figures also show two characteristics, departing from the end points of the initial strip. Furthermore, Figure 28 shows r to be continuous but nonsmooth (left), and its derivative r_y to be discontinuous (right). This is to be expected as the second derivatives r, s, t correspond to a and b via (49), while roughly speaking the derivatives of r, s, t correspond to the derivatives of a, b and f .

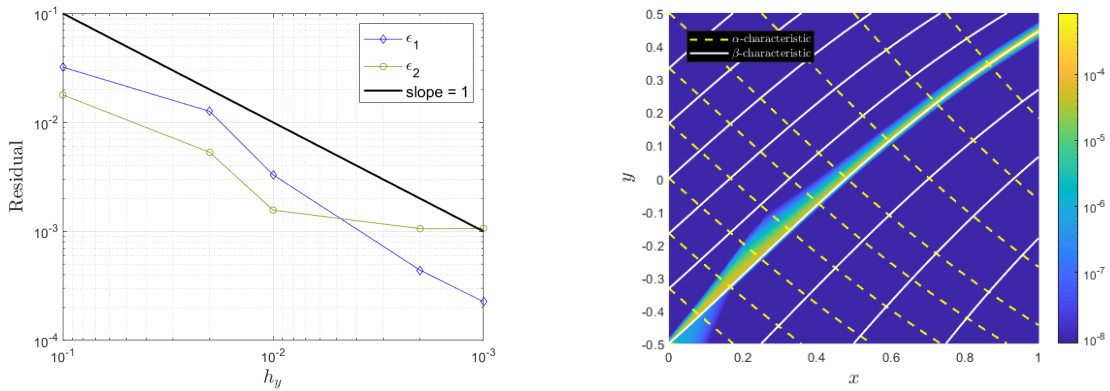


Figure 26: Convergence of the residual (left) and a heat map of the residual ϵ_1 (right) for nonsmooth boundary value a .

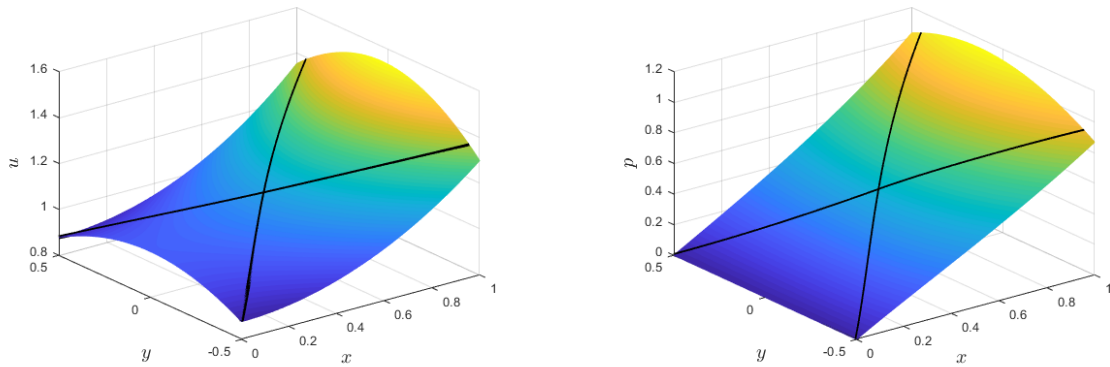


Figure 27: Smooth solutions u (left) and p (right) for nonsmooth boundary data.

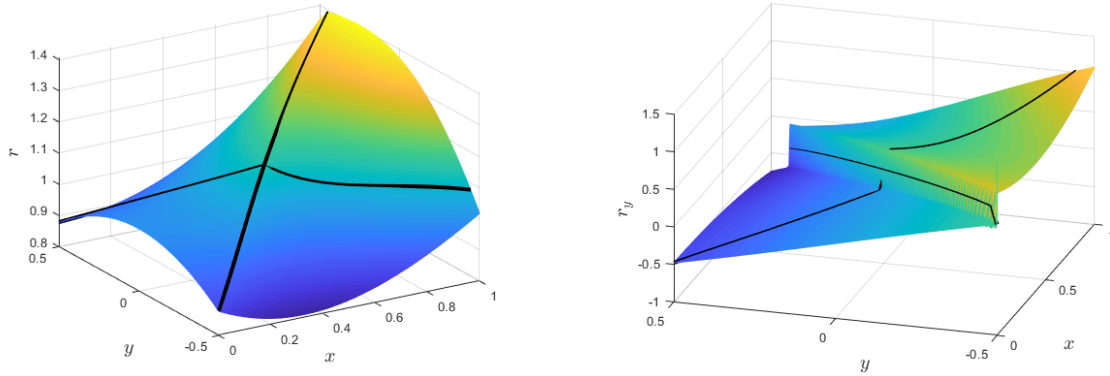


Figure 28: Nonsmooth solutions r (left) and its derivative r_y (right) for nonsmooth boundary data.

6 Conclusions

In this paper, we presented the general formulation of the method of characteristics for a nonlinear second order hyperbolic partial differential equation (PDE) in two variables. We derived conditions which determine whether a curve is characteristic. Along these characteristics the PDE reduces to two systems of ordinary differential equations which are mutually coupled. These ODE systems can be solved using explicit numerical integrators. We presented three such integrators, which are based on one-step methods. The computed characteristics will not pass through grid points. Therefore interpolation is necessary which should be handled carefully as not to spoil numerical convergence. We discussed how the direction of the characteristics at the boundary determines the number of boundary conditions which should be prescribed.

For test cases with known analytical solutions the developed methods are shown to converge to the analytical solution up and till computer precision. Furthermore, two measures for the residual are formulated which seemingly converge to computer precision. The method is shown to work for an example where the initial strip is extended over two boundary segments, and for another example for which the number of boundary conditions necessary vary along a boundary segment. A nonsmooth boundary condition was imposed to show the propagation of the nonsmooth boundary data along the characteristics while the algorithm remained stable.

In future work we would like to extend the algorithm to more general variants of the Monge-Ampère equation. We intend to use the numerical methods to design hyperbolic optical freeform surfaces as has been done in [4] for the elliptic Monge-Ampère equation.

References

- [1] M. N. Koleva and L. G. Vulkov. Numerical solution of the Monge-Ampère equation with an application to fluid dynamics. *AIP Conference Proceedings*, 2048(1):030002, 2018.

- [2] A. Caboussat. Computation of portfolio hedging strategies using a reduced Monge-Ampère equation. In Proceedings of the 20th International Conference on Computing in Economics and Finance, Oslo, June 22-24, 2014, pages 1–13, 2014.
- [3] T. Chen. Smooth local solutions to degenerate hyperbolic Monge-Ampère equations. Annals of PDE, 5(1):1–47, Jan 2019.
- [4] C. R. Prins. Inverse Methods for Illumination Optics. PhD thesis, Eindhoven University of Technology, 2014.
- [5] N. K. Yadav, L. B. Romijn, J. H. M. ten Thije Boonkamp, and W. L. IJzerman. A least-squares method for the design of two-reflector optical systems. Journal of Physics: Photonics, 1(3):034001, Jul 2019.
- [6] L. B. Romijn, J. H. M. ten Thije Boonkamp, and W. L. IJzerman. Freeform lens design for a point source and far-field target. Journal of the Optical Society of America A, 36(11):1926, Nov 2019.
- [7] L. B. Romijn, J. H. M. ten Thije Boonkamp, M. J. H. Anthonissen, and W. L. IJzerman. An iterative least-squares method for generated Jacobian equations in freeform optical design. SIAM Journal on Scientific Computing, 43(2):B298–B322, Jan 2021.
- [8] F. Brickell and B. S. Westcott. Reflector design for two-variable beam shaping in the hyperbolic case. Journal of Physics A: Mathematical and General, 9(1):113–128, Jan 1976.
- [9] B. S. Westcott and F. Brickell. Computation of reflector surfaces for two-variable beam shaping in the hyperbolic case. Journal of Physics A: Mathematical and General, 9(4):611–625, Apr 1976.
- [10] J. Hong. The global smooth solutions of Cauchy problems for hyperbolic equation of Monge-Ampère type. Nonlinear Analysis: Theory, Methods & Applications, 24(12):1649–1663, Jun 1995.
- [11] D. V. Tunitsky. On global solvability of initial value problem for hyperbolic Monge-Ampère equations and systems. Doklady Mathematics, 96(1):377–379, Jul 2017.
- [12] R. M. M. Mattheij, S. W. Rienstra, and J. H. M. ten Thije Boonkamp. Partial Differential Equations: Modeling, Analysis, Computation. Society for Industrial and Applied Mathematics, 2005.
- [13] A. Adams and C Essex. Calculus: a complete course (7th Ed.). Pearson, 2009.
- [14] R. Courant and D Hilbert. Methods of Mathematical Physics: Partial Differential Equations. John Wiley & Sons, Ltd, Apr 1989.
- [15] S. J. Leon. Linear Algebra with Applications (9th Ed.). Pearson, 2015.
- [16] K. Höllig and J. Hörner. Approximation and Modeling with B-Splines. Society for Industrial and Applied Mathematics, Philadelphia, PA, 2013.
- [17] K. Toraichi, K. Katagishi, I. Sekita, and R. Mori. Computational complexity of spline interpolation. International Journal of Systems Science, 18(5):945–954, 1987.
- [18] W. Gautschi. Numerical Analysis (2nd Ed.). Birkhäuser Basel, 2012.

- [19] A.H. Stroud and D. Secrest. Gaussian Quadrature Formulas: By A.H. Stroud and Don Secrest. Prentice-Hall series in Automatic Computation. Prentice-Hall, 1966.
- [20] D. Kahaner, C.B. Moler, G.E. Forsythe, S. Nash, S.G. Nash, and M.A. Malcolm. Numerical Methods and Software. Prentice-Hall series in Computational Mathematics. Prentice Hall, 1988.
- [21] Y. S. Volkov. Study of the convergence of interpolation processes with splines of even degree. Siberian Mathematical Journal, 60(6):973–983, Nov 2019.

Appendices

A Interpolation

In this section we will briefly introduce splines, which we use for numerical interpolation. To understand spline interpolation, we first introduce knot sequences, which generate B-splines, and in term determine the spline interpolant. To this end consider a set of $N + 1$ numbers $\boldsymbol{\xi} = \{\xi_0, \xi_1, \dots, \xi_N\}$ with $\xi_0 \leq \xi_1 \leq \dots \leq \xi_N$. Such a sequence is called a knot sequence and each member of the sequence is called a knot. B-splines b_k^n of degree n for the knot sequence $\boldsymbol{\xi}$ are recursively defined on the interval $[\xi_k, \xi_{k+n+1})$ by [16, p. 52]

$$b_k^n(t) = \gamma_k^n(t)b_k^{n-1}(t) + \left(1 - \gamma_{k+1}^n(t)\right)b_{k+1}^{n-1}(t), \quad \gamma_k^n(t) = \frac{t - \xi_k}{\xi_{k+n} - \xi_k}, \quad (101)$$

for $0 \leq k, k + n + 1 \leq N, 0 \leq n \leq k$ with initial values

$$b_k^0(t) = \begin{cases} 1, & \text{if } \xi_k \leq t < \xi_{k+1}, \\ 0, & \text{otherwise.} \end{cases} \quad (102)$$

Each B-spline b_k^n is a polynomial, of degree $\leq n$ on its knot interval $[\xi_k, \xi_{k+n+1})$, and vanishes outside this interval.

Let $m \in \mathbb{N}_+$, let g be a sufficiently smooth function and let $t_0 \leq \dots \leq t_{m-1}$ be a set of points such that $g(t_0), \dots, g(t_{m-1})$ are known. Furthermore, let $N = m + n$, so $\boldsymbol{\xi} = \{\xi_0, \xi_1, \dots, \xi_{m+n}\}$ and let $\boldsymbol{\xi}$ be such that

$$\xi_k < t_k < \xi_{k+n+1} \text{ for } k = 0, \dots, m - 1. \quad (103)$$

These conditions, also known as the Schoenberg-Whitney conditions [16, p. 91], imply that there exists a unique interpolating spline

$$P(t) = \sum_{k=0}^{m-1} c_k b_k^n(t), \quad (104)$$

of degree n , which interpolates g in the interval $t \in [t_0, t_{m-1})$. The coefficients c_k are calculated via the implicit relation

$$\mathbf{A}\mathbf{c} = \mathbf{g}, \quad (a_{j,k}) = b_k^n(t_j), \quad \mathbf{c} = (c_k), \quad \mathbf{g} = (g(t_k)), \quad (105)$$

for $j, k = 0, 1, \dots, m - 1$. Furthermore, the associated error can be estimated by

$$|g(t) - P(t)| \leq C \left(n, \|\mathbf{A}^{-1}\|_{\infty} \right) \|g^{(n+1)}\|_{\infty, R} h^{n+1}, \quad t \in R, \quad (106)$$

where $\|g^{(n+1)}\|_{\infty, R}$ is the maximum norm of the derivative of g of order $n + 1$ on the interval $R = [\xi_n, \xi_{n+m}]$, $h = (\xi_{j+1} - \xi_j)$ and the constant C depends on the degree n of the B-splines and the infinity-norm of the inverse of \mathbf{A} . A convergence order for odd and even n has been established, where generally convergence for odd n is of order $\mathcal{O}(h^{n+1})$ as given by (106). Convergence for even n has been observed to be of order $\mathcal{O}(h^{n+2})$ instead of the theoretical established upper bound (106). This observed superior convergence for even n is not fully understood at the time of writing [21].

What remains is to construct a suitable knot sequence such that the Schoenberg-Whitney condition holds. Let data points $t_0 \leq \dots \leq t_{m-1}$ be such that $m > n$, i.e., let the number of data points exceeds the degree of the B-splines used for interpolation. Then we choose the knot sequence $\boldsymbol{\xi}$ according to

$$\begin{cases} \xi_i = t_0 & i = 0, \dots, n - 1, \\ \xi_i = \frac{1}{n-1} \sum_{j=1}^{n-1} t_{i-n+j}, & i = n, \dots, m, \\ \xi_i = t_m & i = m + 1, \dots, m + n - 1. \end{cases} \quad (107)$$

The first and last terms of $\boldsymbol{\xi}$ are the original, possibly duplicated, starting and end values t_0 and t_m , respectively. The remaining components are running averages of size $n - 1$ of $\{t_j\}$, which ensures (103) holds.

Example: Consider the ordered sequence of data points $t : \{1, 2, 4, 5, 7, 10\}$ and let the desired spline order be $n = 3$. Hence $m = 6$ and the knot sequence $\boldsymbol{\xi}$ according to (107) is given by $\xi : \{1, 1, 1, 3, 4.5, 6, 10, 10, 10\}$.

In the case that we require extrapolation at a point $t_e < t_0$ or $t_e > t_{m-1}$, we simply estimate $g(t_e) \approx P(t_e)$. This need for extrapolation does occur for both the modified Euler and Runge-Kutta based methods, as shown in Figure 29 for the modified Euler scheme, due to the predictor lying outside of Ω and missing either the value a , or b , as it cannot be determined along the characteristic. Let without loss of generality $a > b$, then in order to approximate $b(x_{i+\frac{1}{2}}, \tilde{y}_{i+\frac{1}{2}}^{\beta}(1))$ which is needed to calculate $\tilde{\mathbf{v}}_{i+1}^{\beta}(1)$ according to (66), we extrapolate using a spline based on $\tilde{\mathbf{v}}_{i+1/2}^{\alpha}(1)$ for $j = 1, \dots, m + 1$, known at the y -values $\tilde{y}_{i+\frac{1}{2}}^{\alpha}(1)$ inside the domain, to $\tilde{y}_{i+\frac{1}{2}}^{\beta}(1)$ outside the domain.

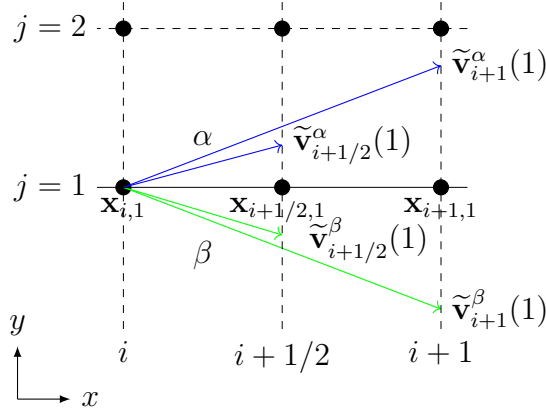


Figure 29: Modified Euler based method near the lower boundary of the domain.

B Generating Solutions to the Hyperbolic Monge-Ampère Equation

Finding solutions to the Monge-Ampère equation can be problematic due to the hyperbolic and nonlinear nature of $u_{xx}u_{yy} - u_{xy}^2 = -f^2 < 0$ with $f \neq 0$. Therefore we introduce a method based on complex functions to quickly obtain a pair (u, f) which solves the Monge-Ampère equation. To this end let w be a complex analytical function and let $u(x, y) = \text{Re}(w(x + iy))$. Differentiation then yields

$$\begin{aligned} u_{xx} &= \text{Re}(w''), \\ u_{xy} &= \text{Re}(iw'') = -\text{Im}(w''), \\ u_{yy} &= -\text{Re}(w''). \end{aligned}$$

For f it then follows

$$f^2 = -u_{xx}u_{yy} + u_{xy}^2 = \left(\text{Re}(w'')\right)^2 + \left(\text{Im}(w'')\right)^2 = |w''|^2.$$

The implications of this are twofold. First, given w we can construct $u(x, y) = \text{Re}(w(x + iy))$ and $f(x, y) = |w''(x + iy)|$, which form a solution. Secondly, if for given f there exists an analytical function w such that $f^2(x, y) = |w''|^2$, then $u(x, y) = \text{Re}(w(x + iy))$ solves the Monge-Ampère equation.

Alternatively, considering $u(x, y) = -\text{Re}(w(x + iy))$ or $u(x, y) = \pm \text{Im}(w(x + iy))$ instead, yields the same conclusions as above.

Acknowledgments

Special thanks goes to J. de Graaf, for contributing App. B, which has greatly simplified generating test examples for the Monge-Ampère equation. Contact: CASA, Department of Mathematics and Computer Science, Eindhoven University of Technology, PO Box 513, 5600MB Eindhoven, The Netherlands

This work is part of the research programme NWO-TTW Perspectief with project number P15-36, which is (partly) financed by the Netherlands Organisation for Scientific Research (NWO).